1-1990

Chromospheric CA II H and K and H alpha Emission in Single and Binary Stars of Spectra Types F6--M2

Klaus G. Strassmeier
Vanderbilt University

Francis C. Fekel
Tennessee State University

Bernard W. Bopp
University of Toledo

Robert C. Dempsey
University of Toledo

Gregory W. Henry
Tennessee State University

THE ASTROPHYSICAL JOURNAL SUPPLEMENT SERIES, 72:191–230, 1990 January

CHROMOSPHERIC Ca II H AND K AND Hα EMISSION IN SINGLE AND BINARY STARS OF SPECTRAL TYPES F6–M2

KLAUS G. STRASSMEIER[1] AND FRANCIS C. FEKEL[1]
Department of Physics and Astronomy, Vanderbilt University
BERNARD W. BOPP[1]
Dominion Astrophysical Observatory, Herzberg Institute of Astrophysics, National Research Council of Canada; and Department of Physics and Astronomy, University of Toledo
ROBERT C. DEMPSEY
Department of Physics and Astronomy, University of Toledo
AND
GREGORY W. HENRY
McDonald Observatory, University of Texas at Austin; and Center of Excellence in Information Systems Engineering, Tennessee State University
Received 1989 April 7; accepted 1989 July 5

ABSTRACT

We have obtained high- and medium-resolution Ca II H and K and/or Hα line profiles for 100 single and binary stars of spectral type F6 to M2 and luminosity class III, IV, and V. The sample includes inactive single and binary stars as well as moderately to extremely active single stars including the FK Com stars and active binary stars of the RS CVn and BY Dra class with a total range of rotation periods from 0.5 to 310 days. A total of 444 spectra have been acquired and are used to measure absolute Ca II H and K emission-line surface fluxes and Balmer Hα core emission equivalent widths. Some of the stars also have been observed at 6430 Å to determine their rotational velocities. These data, supplemented by published observations, have been used to identify correlations between chromospheric activity at Ca II H and K and Hα and effective surface temperature and rotation. Several new stars with chromospheric Ca II H and K emission have been discovered. We have also used ultraviolet C IV emission-line fluxes taken from the literature and compared them with the present data.

No single activity-rotation relation can be derived for all luminosity classes, and there is clear evidence that evolved stars are generally more active than main-sequence stars of the same rotation period. Binarity per se within the evolved stars plays apparently no role, while the main-sequence binary stars show generally higher levels of activity than their single counterparts. Chromospheric emission in the Ca II H and K lines depends also upon surface temperature in the sense that the flux declines with cooler temperature. The trend in the Hα equivalent width–log $\mathscr{F}'$(Ca II K) plane is that with increasing K line flux the Hα absorption core first *deepens* until log $\mathscr{F}'$(K) ~ 5.8 ergs cm^{-2} s^{-1} is reached and then *fills in* quite rapidly.

Subject headings: Ca II emission — line profiles — stars: binaries — stars: chromospheres — stars: emission-line — stars: late-type — stars: rotation

I. INTRODUCTION

Over 70 years ago, Eberhart and Schwarzschild (1913) discovered bright emission lines in the cores of the strong Ca II absorption features of α Boo, α Tau, and σ Gem. Further observations by several authors (e.g., Deslandres and Burson 1922; Wellmann 1940) revealed H_3 and K_3 absorption reversals on top of the H_2 and K_2 emission lines, strengthening the analogy between solar and stellar phenomena.

Efforts to detect active regions from rotational modulation have focused on single main-sequence stars (Vaughan and Preston 1980; Duncan 1981; Baliunas *et al.* 1983; Soderblom 1985; and others). Only a few attempts have been made to see if rapidly rotating single subgiants and giants differ in their chromospheric behavior if compared with (*a*) main-sequence stars with the same rotation rates and effective temperatures (e.g., Rutten 1987) and (*b*) with a similar star in a binary system (e.g., Basri, Laurent, and Walter 1985; Basri 1987; Simon and Fekel 1987). Moreover, the latter studies are based mainly on *ultraviolet* emission lines.

The activity in classes of stars such as the RS CVn binaries and the BY Dra variables is at least one order of magnitude greater than that of our Sun. The stellar parameters of these systems have been summarized in a catalog of chromospherically active binary stars (= CABS; Strassmeier *et al.* 1988). *Absolute* Ca II H and K emission-line fluxes and Hα *core emission* equivalent widths for these stars rarely were determined. One reason for this might be the complication in the analysis due to the binary nature of these stars, that is, e.g., the (presumably unknown) contamination of the emission by the secondary component or the presence of a continuum of a

[1]Visiting Astronomer, Kitt Peak National Observatory, operated by the Association of Universities for Research in Astronomy, Inc., under contract with the National Science Foundation.

hot component which dilutes the emission from the primary. Recent Ca II H and K observations focused almost exclusively on *single* stars, e.g., Linsky *et al.* (1979), 43 stars; Worden, Schneeberger, and Giampapa (1981), 17 stars; Giampapa *et al.* (1981), seven stars; Bopp (1983), 19 stars; Bopp (1984), 14 stars; Fernández-Figueroa *et al.* (1986*b*), seven stars; and most recently Pasquini, Pallavicini, and Pakull (1988), 50 stars. A more detailed investigation of subgiants and giants in binary systems seemed to be needed.

Several authors noted significant filling in of the cores of Hα in very active binary stars (Smith and Bopp 1982; Fekel, Moffett, and Henry 1986) as well as in relatively young Hyades stars (Cayrel *et al.* 1983) and other solar-type dwarfs (Herbig 1985). Chromospheric activity is therefore also established by the presence of emission in the core of the Hα line. While the dwarf stars in the sample of 85 stars of spectral type F8 and later of Zarro and Rogers (1983) showed the same brightening of the Hα core (increasing R_c) with increasing Ca II K emission, the giants tended to have *deeper* Hα cores. From a sample of eight short-period RS CVn and W UMa stars, Barden (1985) found a possible correlation of Hα emission and Rossby number (the ratio between the rotational period and the convective time scale).

In this paper we present new observations of the Ca II H and K and Hε region and/or the Balmer Hα line for a total of 100 mostly very active stars but also for weak or inactive stars which had suspected activity. With the exception of most of the Hα reference stars, almost all of the program stars have been observed at Ca II *and* Hα. Note that the Ca II and Hα observations were not simultaneous. The data were obtained with a variety of telescopes between 1981 and 1989. Our primary goal is to present a set of high-resolution (0.18–0.3 Å) and medium-resolution (0.5–0.9 Å) spectra which will serve the needs described. In addition we will try to verify some trends that may be present. In § II we describe the instrumentation, and in § III we discuss the analysis techniques applied. The spectra are described in § IV, and in § V we discuss systematic trends in the line fluxes and equivalent widths. Appendix A contains a short summary of previously published absolute H and K fluxes for active stars which were included in some of the graphs in § V. Individual Ca II H and K region plots for our program stars are given in Appendix B.

II. INSTRUMENTATION

a) *Calcium* H *and* K

Two telescopes have been used; the Kitt Peak National Observatory's (KPNO) 0.9 m coudé feed telescope and the Dominion Astrophysical Observatory's (DAO) 1.8 m telescope. Table 1 is a summary of the different telescope-spectrograph-detector combinations.

The KPNO data were obtained in the course of three observing intervals in 1987 December, 1988 March, and 1988 May. The coudé spectrograph was used in third order with grating A and camera 5 at a reciprocal dispersion of 4.7 Å mm^{-1}. The observations in December utilized a 512×512 pixel Tektronix CCD and had a 2-pixel resolution of 0.24 Å and a wavelength coverage of 65 Å. For the March and May data we used a 800×800 pixel Texas Instruments (TI-3) CCD and a slightly larger slit width resulting in an effective resolution of 0.3 Å and a wavelength coverage of 56 Å. All observations were centered on 3950.0 Å. The integration times and signal-to-noise (SNR) ratios varied from 1 minute and SNR ≈150 (at the K line bottom) for β Gem, to 90 minutes and SNR ≈ 50 for HD 65195.

The DAO data set was obtained during three observing intervals; 1987 December, 1988 March/April, and 1988 May with the Cassegrain spectrograph fed by the 1.8 m telescope. The observations in December were obtained with a 1872 pixel Reticon array and had a spectral resolution of 0.5 Å. The March and April observations utilized a 512×512 pixel RCA CCD and had, combined with the slightly larger slit width, a resolution of 0.9 Å. The same chip was used for the

TABLE 1
TELESCOPE-SPECTROGRAPH-DETECTOR COMBINATIONS

Year and Month	Telescope	Spectrograph	Detector	Dispersion (Å mm^{-1})	Resolution (Å)	Code
			Ca II H and K			
1987 Dec	KPNO CF	Coudé	TEK CCD	4.7	0.24	KPNO0.24
1988 Mar, May	KPNO CF	Coudé	TI-3 CCD	4.7	0.30	KPNO0.30
1987 Dec	DAO 1.8 m	Cassegrain	Reticon 1872	15	0.5	DAORET0.5
1988 Mar, Apr	DAO 1.8 m	Cassegrain	RCA CCD	15	0.9	DAOCCD0.9
1988 May	DAO 1.8 m	Cassegrain	RCA CCD	15	0.5	DAOCCD0.5
			Hα			
1986 Feb, May	McDonald 2.1 m	Coudé	Reticon 1728	9.5	0.28	2.1McD0.28
1983 Apr, Aug	McDonald 2.1 m	Coudé	Reticon 1728	9.5	0.42	2.1McD0.42
1981 Jan, May	McDonald 2.7 m	Coudé	Reticon 1024	4.4	0.35	2.7McD0.35
1989 Jan	KPNO CF	Coudé	TI-3 CCD	7.6	0.21	KPNO0.21
1988 May	KPNO CF	Coudé	TI-3 CCD	7.6	0.18	KPNO0.18
1985 Sep, Oct, Nov	KPNO CF	Coudé	TI-3 CCD	7.6	0.2	KPNO0.2
1985 Mar	KPNO CF	Coudé	TI-3 CCD	15	0.4	KPNO0.4
1985 Mar	KPNO CF	Coudé	RCA CCD	7.6	0.5	KPNO0.5
1986 Apr–1988 Sep	Ritter 1 m	Echelle	Reticon 1024	2.5	0.3	Ritter0.3

May observations, but with effective wavelength resolution of 0.5 Å. The signal-to-noise ratios are in the same range as the KPNO data.

Both data sets were reduced in the standard fashion using the Image Reduction and Analysis Facility's (IRAF)[2] subpackage for CCD Spectra (Pilachowski and Barnes 1987) available at KPNO and DAO.

b) *Balmer* Hα

These observations were obtained at three different observatories: McDonald Observatory, University of Texas, using mostly the 2.1 m telescope; KPNO using the coudé feed telescope; and Ritter Observatory, University of Toledo, using the 1 m reflector.

A few spectra were obtained with the 2.7 m McDonald telescope and a 1024 pixel Reticon array at a resolution of 0.35 Å as early as 1981. The vast majority, however, was taken with the 2.1 m in 1983 and 1986. These observations utilized the coudé spectrograph with grating 2 in first order and the 1872 pixel Reticon and had a dispersion of 9.5 Å mm^{-1} covering a wavelength region of approximately 265 Å. For the 1983 data we used a 90 μm slit achieving a spectral resolution of 0.42 Å, whereas the 1986 observations were made with a 60 μm wide slit resulting in a somewhat better resolution of 0.28 Å. The SNRs for all three data sets were in the range 50–200:1 with most around 100:1.

The Ritter data were obtained between 1986 and 1988 with the 1 m telescope and a fiber-fed echelle spectrograph at a reciprocal dispersion of 2.5 Å mm^{-1}. The detector was an intensified 1024 pixel Reticon array (Bopp, Dempsey, and Maniak 1988), which when combined with a relatively large slit width in order to decrease integration time resulted in a spectral resolution of 0.3 Å. The wavelength coverage was 60 Å centered on 6570 Å. The SNRs for these observations are in the range of 50–150:1.

Higher resolution scans were obtained in 1988, and 1989 with the KPNO coudé feed telescope using camera 5 and grating A in second order. The dispersion of 7 Å mm^{-1} and the TI-3 CCD pixel size of 15 μm resulted in a 2-pixel spectral resolution of 0.18 Å while covering a 84 Å field centered on Hα. The obtained SNR is approximately 150:1. The 1985 runs utilized camera 5, grating B or D, and the TI-3 or RCA CCD at resolutions between 0.2 and 0.5 Å.

III. DESCRIPTION OF MEASURED PARAMETERS

a) *Absolute* Ca II H *and* K *Surface Flux*

Our measurements of the surface flux in ergs cm^{-2} s^{-1} followed the procedures outlined by Linsky *et al.* (1979). Willstrop (1964) obtained absolutely calibrated 50 Å bandpass photometry for stars of various spectral types and luminosity classes. Barnes and Evans (1976) have shown that the angular diameter of a star may be derived from its $V-R$ color and apparent visual brightness. Linsky *et al.* used this relation to convert Willstrop's 3925–3975 Å fluxes into absolute surface fluxes and plotted them versus the $V-R$ color and found a tight correlation with only 1.4% average deviation. A piecewise linear least-squares fit to these data describes then the relationship between the stellar flux per angstrom, $\mathscr{F}$, in the 3925–3975 Å bandpass and the $V-R$ color

$$\log \mathscr{F} = 8.264 - 3.076(V-R) \quad \text{for } V-R<1.3. \quad (1)$$

Knowing the $V-R$ color of a stars one can derive its stellar surface continuum flux in ergs cm^{-2} s^{-1} $Å^{-1}$ in the 3925–3975 Å bandpass. Thus, all Ca II H and K spectra for which this calibration may be applied must contain this 50 Å bandpass centered on 3950 Å.

The H and K emission-line fluxes are derived by setting the measured relative fluxes, $f(\Delta\lambda)$, equal to the calibrated flux so that

$$\mathscr{F}(H_1; K_1) = \frac{50\mathscr{F}}{f(\Delta\lambda = 50\ \text{Å})} f(H_1; K_1), \quad (2)$$

where the observed fluxes are always measured from the zero-flux level. This is demonstrated in Figure 1 where the bottom line of the graph shall represent the zero-flux level. While this calibration technique places all stars on a uniform flux scale for intercomparison there are still several problems which may be noted:

1. The emission-line surface fluxes, also called the K_1 and H_1 *indices*, are defined as the flux above the zero-flux level and between (e.g., for the K line) the K_{1V} and K_{1R} minima, as illustrated in Figure 1. Our measurements of, e.g., $\Delta\lambda(K_1) = \lambda(K_{1R}) - \lambda(K_{1V})$ (Table 4) showed internal errors of up to 9%, or approximately 6% in the resulting flux, depending on how well the minima were defined and therefore depending on the instrumental resolution.

2. If the observed $B-V$ of a chromospherically active (CA) star is matched with the appropriate value of the intrinsic color in Johnson's (1966) tables, the CA stars show $V-R$ and $V-I$ color excesses of 0.06–0.10 mag (Fekel, Moffett, and Henry 1986) while dark starspots normally account only for $V-R$ changes of ≤ 0.03 mag (an exception might be II Peg where a big spot in 1977 produced $V-R$ *variations* of 0.066 mag; Vogt 1981). Moreover, several of our program stars have never been observed in R and therefore have no observed $V-R$ color. To be on a consistent scale throughout this paper we decided to use Johnson's (1966) spectral type–$V-R$ color relation for the flux calibration procedure. Whenever possible we used the spectral types given in the CABS catalog or, especially for the single stars, we used the classifications listed in Keenan (1983) and Fekel, Moffett, and Henry (1986). These $V-R$s are listed in Table 2. Recently, Soderblom (1989) presented evidence that the color "anomalies" of active Hyades stars (Campbell 1984) are not real but due to duplicity which might justify the use of *theoretical* colors instead of observed.

3. The integral, $f(\Delta\lambda = 50$ Å$)$, in the denominator in equation (2) *includes* the H and K emission features but the calibration of $\mathscr{F}(\Delta\lambda = 50$ Å$)$ is derived from the Willstrop stars which were selected without much regard to their H and K characteristics.

[2]IRAF is distributed by National Optical Astronomy Observatories, which is operated by the Association of Universities for Research in Astronomy, Inc., under contract with the National Science Foundation.

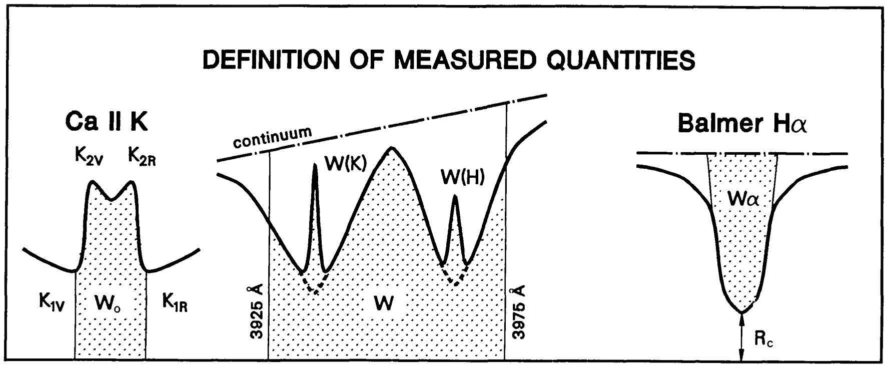

FIG. 1.—Definition of measured quantities. *Left graph:* The red (R) and violet (V) K_1 points of the central Ca II K emission determine the wavelength boundaries for our flux integration (dotted area labeled W_0). The graph bottom indicates the zero-flux level. The K_{2R} and K_{2V} points, produced by the line reversal in the emission center, mark the strength of the emission line above the pseudocontinuum (i.e. the dashed lines shown in the middle graph). *Middle graph:* Shown are the integration boundaries of the $\Delta\lambda = 50$ Å bandpass needed for the flux calibration procedure. W(K) and W(H) are the equivalent widths of the K and H emission lines measured above the pseudocontinuum (*dashed lines*), while W is the "equivalent width" within the 50 Å bandpass (*dotted area*) including W(K) and W(H). *Right graph:* Definition of the Hα "equivalent width" term used throughout this paper.

In the case of very active stars, like the RS CVn binaries, point (3) might be significant. To see to what extent this would influence the emission-line fluxes we reduced the 0.24 Å resolution KPNO data also in a slightly different way; namely, measuring actual equivalent widths (EW) and subtracting the H and K *emission* EW measured from the pseudocontinuum, i.e., W(K) and W(H) in the middle panel of Figure 1, from the EW of the 50 Å bandpass, labeled W in Figure 1, resulting in

$$\mathscr{F}(H_1; K_1) = \frac{50\mathscr{F}}{W - W(K) - W(H) - W(H\varepsilon)} W_0(H; K). \quad (3)$$

The quantities W_0(K), W_0(H), W(K), W(H) and W(Hε) are listed in Table 4. Even in stars with *emission* equivalent widths of >1 Å, the differences in the absolute line fluxes are generally less than 10% but can reach up to approximately 15% in the case of HD 106225 [W(K) ≈ 2.2 Å]. A particular problem with this method is the determination of the continuum. This is demonstrated in the middle graph of Figure 1.

The absolute fluxes of stars which have been observed at KPNO and at DAO are compared in Figure 2*a*. Their mean deviation is within the expected range of the external error of approximately 20%. Figure 2*b* compares our H_1 and K_1 indices with those of other authors. The agreement is mostly better than ≈ 40% taking into account that the data have been obtained at different epochs, which is important because most of our program stars are supposed to be intrinsically variable. We estimate the internal precision of both data sets (KPNO and DAO) to be ≈15%, and the external accuracy (KPNO vs. DAO) to be slightly better than ≈ 20%.

b) H *and* K *Line Radiative Losses*

After the absolute surface fluxes in the cores of the H and K lines have been determined, the flux which rises from the underlying photosphere must be subtracted. As demonstrated

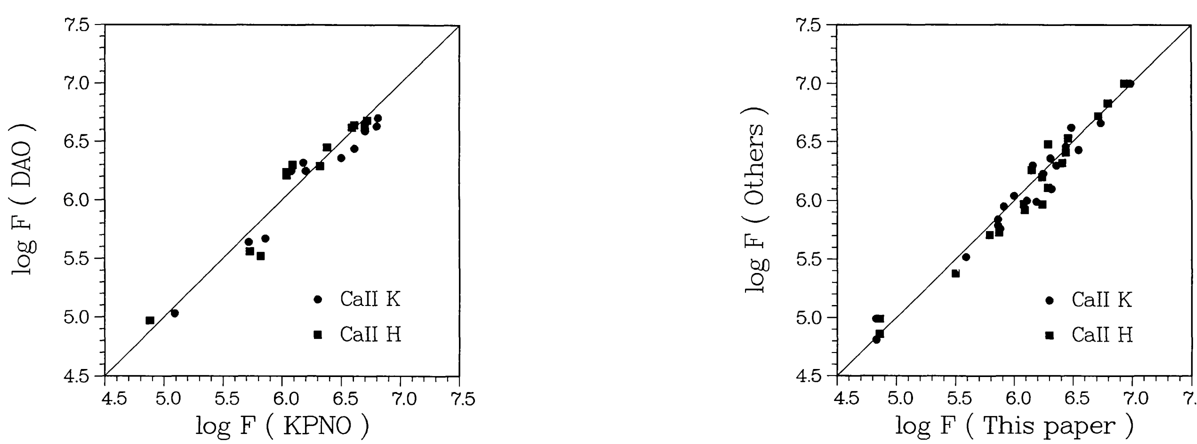

FIG. 2.—*Left panel:* Comparison of the KPNO fluxes with those from DAO. *Right panel:* Comparison of the KPNO and DAO fluxes from this paper with those from other authors (Table 7).

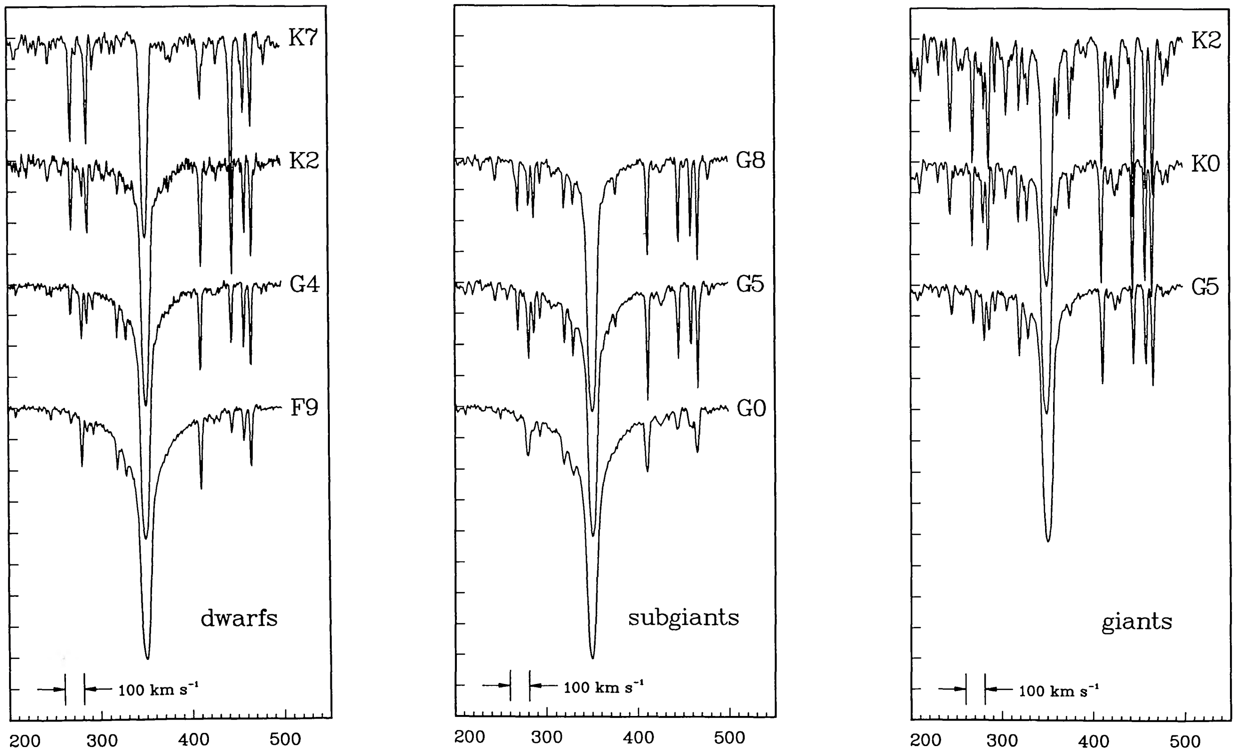

FIG. 3*a* FIG. 3*b* FIG. 3*c*

FIG. 3.—Hα profiles for 10 reference absorption-line stars. (*a*) Dwarfs; (*b*) subgiants; (*c*) giants. All 10 observations were made with the KPNO coudé feed telescope at a resolution of 0.18 Å. The spectra are shifted in intensity for better display. The ordinate is in pixels with an arbitrary velocity range of 100 km s^{-1} (~ 2 Å) indicated. Note the increasing Hα wings with hotter spectral type.

by Linsky and Ayres (1978), the resulting excess flux is the net chromospheric radiative loss in the H and K lines, respectively. Linsky *et al.* (1979) also present H_1 and K_1 indices for radiative equilibrium model atmospheres (i.e., no chromosphere), $\mathscr{F}_{RE}(H_1)$ and $\mathscr{F}_{RE}(K_1)$, which can be used to derive the radiative losses in the H and K lines represented by the corrected H_1 and K_1 indices $\mathscr{F}'(H_1)$ and $\mathscr{F}'(K_1)$

$$\mathscr{F}'(H_1; K_1) = \mathscr{F}(H_1; K_1) - \mathscr{F}_{RE}(H_1; K_1) . \quad (4)$$

These excess fluxes are listed in Table 3 along with the uncorrected fluxes.

c) Hα *Core Emission Equivalent Widths*

The Hα core emission was determined by subtraction of the equivalent width of a presumably inactive star of the same spectral type and luminosity class. Shown in Figure 3 are some of the reference star spectra. Table 5 lists the equivalent widths and residual intensities of the reference stars. In most cases the program star and the reference star were observed several times. If so, we used their mean values in the analysis.

The core emission equivalent width was measured following the precepts of Bopp, Dempsey, and Maniak (1988). This is schematically illustrated in the right section of Figure 1. First, we established the continuum intensity above the Hα core by searching for the five to 10 highest counts per pixel in two relatively line-free 3 Å windows centered at 6540 and 6590 Å. A straight line was then drawn between these two points. Second, extending the sides of the absorption profile in a straight line to the continuum level results in the limits of integration for the equivalent width. This technique nearly eliminates the contamination by nearby water vapor lines, the uncertainties of the sometimes very broad Hα wings and, in addition, concentrates on the core of the line where chromospheric emission should be first visible.

This artificial "equivalent width" however *depends* on the $v \sin i$ of the star. Therefore, all reference spectra were first rotationally broadened with the appropriate value of $v \sin i$ of the program star and then subtracted from each other. With the nomenclature in Figure 1 we followed

$$\langle W_{em} \rangle = \langle W_{\alpha}(\text{program star}) \rangle - \langle W_{\alpha}(\text{broad. ref. star}) \rangle . \quad (5)$$

The angle brackets denote mean values for the cases where more than one spectrum was obtained. These values are listed in Table 6A with their respective standard deviations. If $\sigma_{W\alpha} \geq 0.060$ Å, we considered the star to have an intrinsically variable Hα profile and listed the individual results in Table 6B. Also listed are the residual intensities, R_c, measured from zero intensity to the line bottom.

The internal precision of the "equivalent width" for spectra of reference stars taken on the same night is approximately 4 mÅ for the Kitt Peak coudé feed data, 6 mÅ for the 2.1 m

McDonald data, and 10 mÅ for the Ritter data. The external accuracy for the core emissions estimated from spectra taken at different epochs, however, has a greater range with a mean of ≈ 40 mÅ. Some of the stars in Table 6B have been observed with different telescope-spectrograph configurations with approximately the same resolution. The external accuracy for these observations is of course somewhat larger, say ≈ 60 mÅ. The equivalent widths from the 0.18 Å KPNO coudé feed spectra agree generally to within a few percent with the 0.28 Å McDonald spectra—with one exception, though, i.e., β Vir, where the McDonald value is 9% larger. The 0.42 Å McDonald equivalent widths are consistently ≈ 5% larger than the 0.18 Å KPNO data, while the 0.3 Å Ritter Observatory echelle equivalent widths are ≈ 10% larger than a corresponding coudé observation. There is again one exception: η Boo, the only Hα reference star with significantly broadened lines ($v \sin i = 11$ km s^{-1}), where the Ritter value exceeds the 0.18 Å KPNO value by 25%. Therefore, stars with Hα core emission equivalent widths, $\langle W_{\rm em} \rangle$, less than +0.04 to +0.06 Å should be considered as nonactive or, at most, weakly active. Note that we corrected the Ritter echelle spectra for light scattering in the spectrograph (Bopp, Dempsey, and Maniak 1988) but not the coudé spectra where this problem is less significant.

A number of stars were found to have negative core emission equivalent widths; i.e., even weaker chromospheric emission than the reference star used (compare with Herbig 1985). This may be caused by (a) spectral type mismatches between program star and reference star, (b) an unreliably large value of $v \sin i$ of the program star, (c) the presence of a composite spectrum, and (d) differences of the chromospheric structure among stars with H and K emission. Table 6A contains 11 stars with $\langle W_{\rm em} \rangle < -0.1$ Å. While problem (a) makes the core emission equivalent width either smaller or larger, problems (b), (c), and (d) make it always smaller. Thus, we might expect some unfortunate cases where all of these problems are added together resulting in an unrealistic negative emission value. Although spectral type mismatches can cause spurious "emission" equivalent widths, their upper limit should be smaller than our cutoff value of 0.04–0.06 Å.

d) *Rotational Velocities*

For many of the stars in our sample we were unable to find a value of $v \sin i$ in the literature or the existing values are uncertain upper limits (particularly in the case of some reference stars). Thus, we determined values of the projected rotational velocities (Table 2) for 24 systems, five of which are double-lined.

To determine the rotational velocities, the full width half-maxima (FWHM) of several lines in the 6430 Å region were measured, and the average value determined. The FWHM of comparison-lamp lines were also measured, and the average for these lines was assumed to be the instrumental profile. Such instrumentally corrected FWHM were compared with the line broadening determined from model atmosphere analyses (Vogt 1981) to determine an empirical relationship between these two quantities:

$$v \sin i = 0.591\left\{\left[\frac{c}{\lambda}\left(\mathrm{FWHM}_{\rm obs}^2 - \mathrm{FWHM}_{\rm instr}^2\right)^{1/2}\right]^2 - \zeta^2\right\}^{1/2} \quad (6)$$

The values of $v \sin i$ were determined using equation (6) with an assumed macroturbulence, ζ, of 3 km s^{-1} (Gray 1982), except for those giant stars having spectral types of G5 or earlier for which a macroturbulence of 5 km s^{-1} (Gray 1982) was assumed. The factor 0.591 is from the empirical relationship mentioned above. The rotational velocities have uncertainties of 2–3 km s^{-1}, an estimate based on the consistency of individual widths from line to line, on the reproducibility of results when $v \sin i$ was determined from more than one spectrum, and on the calibration of the system.

IV. INDIVIDUAL RESULTS

A representative example of one Ca II H and K observation for each of the 83 stars listed in Table 3 (including the Sun) is given in Appendix B (Fig. 10). In Table 3 the star's effective temperature is given from the spectral type–temperature relation listed in Landolt-Börnstein (Schmidt-Kaler 1982). Also listed are the uncorrected Hϵ indices, $\log \mathscr{F}(\mathrm{H}\epsilon)$, defined as the total surface flux above the zero-flux level, the uncorrected Ca II H_1 and K_1 indices, $\log \mathscr{F}(\mathrm{K}_1)$ and $\log \mathscr{F}(\mathrm{H}_1)$, the corrected Ca II H_1 and K_1 indices, $\log \mathscr{F}'(\mathrm{K}_1)$ and $\log \mathscr{F}'(\mathrm{H}_1)$, the chromospheric radiative loss normalized to the total surface luminosity of the star, $R_{\rm HK}$, and in the last column a code for the telescope-spectrograph-detector combination explained in Table 1.

Listed in Table 4 are the measured equivalent widths and line widths at different locations in the H and K lines. This table contains only data from the 0.24 Å and 0.3 Å resolution KPNO spectra. The first column lists the equivalent width of the Hϵ emission feature (if present), defined as the equivalent width above the interpolated wing of the Ca II H line (= pseudocontinuum). The other equivalent width measures in this table, $W_0(\mathrm{K;H})$ and $W(\mathrm{K;H})$, are explained in § III and in Figure 1. The $\Delta\lambda_{(\mathrm{K1})}$ width is defined as the wavelength separation between K_{1V} and K_{1R} (Fig. 1), similarly for $\Delta\lambda_{(\mathrm{H1})}$. The $\Delta\lambda_{(\mathrm{K2})}$ and $\Delta\lambda_{(\mathrm{H2})}$ widths are defined as the wavelength separations between the two H_2 and K_2 points, respectively. The last two columns list the full width at half-maximum for the K and H line, FWHM(K) and FWHM(H), and are defined as the full width measured between the flux levels halfway between the mean flux at K_1 and K_2 and H_1 and H_2, respectively. We list these parameters so that they may be used in testing different line formation theories.

Representative Hα region spectra for five stars are shown in Figure 4 along with their respective reference stars. Tables 5, 6A, and 6B summarize the Hα-observation results. Table 5 contains the equivalent widths and residual intensities for the reference stars, while Table 6A lists the values for the active

1990ApJS...72..191S

TABLE 2

PROPERTIES OF OBSERVED STARS

Star Name	HD	Spectral Type (hot/cool)	V (mag)	V-R^c (mag)	P_{rot} [a] (days)	$v \sin i$ (km s^{-1})	Binarity	Active Chromosphere Star ?
δ And	3627	K3III	3.27	0.96	[260]	≤3[b]	SB1	no
HR 166	3651	K0V	5.87	0.64	48:	≤3.7[b]	S	no
AY Cet	7672	WD/G5III	5.47	/0.69	75.12	/4	SB1	yes
HR 339	6903	G0III	5.55	0.51	6.2	91	S	yes
HR 454	9746	gK1	5.92	0.81	76.0	8	S	yes
BD+34°363	12545	G5IV	7.6	0.77	orb23.9	17[b]	SB1	yes
α Ari	12929	K2III	2.00	0.84	[240]	3.1	S	no
VY Ari	17433	K3-4IV	6.87	0.85	17.4	6	SB1	yes
BD+25°497	19485	G4V/G6V	8.36	0.54/0.55	orb6.15	10/6[b]	SB2	yes
HR 1023	21018	G5III	6.38	0.69	[20]	20	SB1	yes
UX Ari	21242	G5V/K0IV	6.5	/0.77	6.44	6/37	SB2	yes
V711 Tau	22468	G5IV/K1IV	5.7	/0.81	2.84	13/38	SB2	yes
10 Tau	22484	F9V-IV	4.28	0.48	[15]	4	S	no
δ Eri	23249	K0+IV	3.54	0.77	[100]	2.2	S	no
HR 1176	23838	G2III	5.66	/0.60	[25]	<11[b]	SB1	yes
V491 Per	25893	G8IV	7.13	0.64	7.5	6	CVB[d]	yes
EI Eri	26337	G5IV	6.95	0.61	1.945	50	SB1	yes
HR 1362	27536	G8IV	6.27	0.64	309.6	6	S	yes
BD+14°690	27691	G0V	7.0	0.50	orb4.00	8[b]	SB1	yes
V492 Per	28591	K1III	6.72	0.81	21.3	24	SB1	yes
HR 1455	29104	F/G5III-II	6.36	/0.69	[150]	/6[b]	SB2	no
BD+26°730	...	dK5e	8.42	0.99	orb1.9	8[b]	SB1	yes
BD+64°487	30957	G8:IV	8.6	0.64	[20]	6/6[b]	SB2	yes
BD+0°908	31738	G5IV	7.13	0.61	4.5	/17	SB2	yes
BD+03°733	31993	K2III	7.53	0.84	13.0	31	S	yes
12 Cam	32357	K0III	6.25	0.77	84.9	15	SB1	yes
BD+47°1117	33798	K0III	7.0	0.77	9.8	29[b]	S	yes
CD-26°2085	34198	K0III	7.1	0.77	28.4	15	S	yes
HR 1908	37171	K4III	5.94	1.06	[300]	<3	SB1	yes
χ¹ Ori	39587	G0V	4.41	0.50	5.10	6	S	yes
HR 2081	40084	G5III	5.89	0.69	orb219.	...	SB2	no
1 Gem	41116	[F6-7/]K0III	4.16	[/]0.77	...	6/6[b]	SB3	no
OU Gem	45088	K3V/K5V	6.79	0.82/	7.36	5.6/5.6	SB2	yes
σ Gem	62044	K1III	4.14	0.81	19.410	25	SB1	yes
κ Gem	62345	G8III	3.57	0.70	[86]	6[b]	S	no
β Gem	62509	K0III	1.14	0.77	[240]	2.5	S	no
BD+42°1790	65195	G5III	9.12	0.69	orb37.9	12[b]	SB1	yes
54 Cam	65626	F9IV/F9IV	6.52	0.50/0.50	10.163	10/14[b]	SB2	yes
28 Mon	65953	K4III	4.68	1.06	[87]	10	S	no
β Cnc	69267	K4III	3.52	1.06	[180]	5[b]	S	no
o UMa	71369	G5III	3.36	0.69	[150]	2.6	S	no
35 Cnc	72779	G0III	6.58	0.51	[2.6]	91	S	no
π¹ UMa	72905	G0V	5.64	0.50	[11]	4	S	yes
Gliese 338 A	79211	M0Ve	7.62	1.28	...	...	CVB[d]	yes
BD+40°2197	80715	K3V/K3V	7.7	0.82/0.82	3.8	10/10	SB2	yes
IL Hya	81410	K1III	7.4	0.81	12.69	22	SB1	yes
24 UMa	82210	G4IV-III	4.56	0.65	(0.92?)	4.9	S	yes
LQ Hya	82558	dK0	7.5	0.64	1.5978	25	S	yes
Gliese 378.1	86856	dK8	9.04	1.20	[7]	4[b]	S	yes
Gliese 380	88230	K7V	6.59	1.15	...	...	S	yes
LR Hya	91816	K0V/K0V	7.58	0.64/0.64	orb6.8	6/6	SB2	yes
Gliese 410	95650	dM2e	9.52	1.50	2.935	...	S	yes
ξ UMa(B)	98230	G5V	4.87	0.54	orb3.980	2.8	SB1	yes
HR 4430	99967	K2III	6.35	0.84	76.6	16[b]	SB1	yes
DF UMa	...	dM0e	10.12	1.28	orb1.033	≤25	SB2	yes
61 UMa	101501	G8V	5.33	0.58	17.1	<15	S	yes
β Vir	102870	F9V	3.61	0.48	[14]	3.2	S	no
BD-8°3301	106225	K0III	8.1	0.77	10.6	25	SB1	yes
31 Com	111812	G0III	4.94	0.51	[4.2]	57[b]	S	yes
ε Vir	113226	G8III	2.83	0.70	...	<15	S	no
BD+57°1417	113983	G8III	7.5	0.70	[80]	6	S	no
β Com	114710	G0V	4.26	0.50	[11]	4	S	no
BD+34°2411	115781	F/K0III	8.13	/0.77	orb18.7	7/35	SB2	yes
BM CVn	116204	K1III	7.21	0.81	20.66	15	SB1	yes
BD+36°2368	116378	G5V	8.87	0.54	orb17.76	≤3[b]	SB1	yes
70 Vir	117176	G4V	4.98	0.54	[37]	1:[b]	S	no
FK Com	117555	G2III	8.2	0.58	2.40	120	S	yes
HR 5110	118216	F2IV/K2IV	4.95	/0.79	orb2.613	/10	SB2	yes
τ Boo	120136	F6IV	4.50	0.40	[7]	14.5	S	no
η Boo	121370	G0IV	2.68	0.50	[10]	11[b]	SB1	no
4 UMi	124547	K3III	4.82	0.96	[160]	5[b]	SB1	no

TABLE 2—*Continued*

Star Name	HD	Spectral Type (hot/cool)	V (mag)	V-R^c (mag)	P_{rot} [a] (days)	$v \sin i$ (km s^{-1})	Binarity	Active Chromosphere Star ?
α Boo	124897	K1III	-0.04	0.81	[280]	2.4	S	no
ρ Boo	127665	K3III	3.57	0.96	[200]	4[b]	S	no
ϵ Boo	129989	K0III-II	2.37	0.77	...	6.6	S	no
HR 5534	130948	G0-2V	5.85	0.50	...	...	S	yes
ξ Boo A	131156	G8V	4.74	0.58	6.2	3	S	yes
ξ Boo B	131156	K4V	6.9	0.91	11.5	...	S	yes
HR 5553	131511	K2V	6.01	0.74	[7.7]	4[b]	SB1	yes
UV CrB	136901	K1III	7.21	0.81	orb18.67	42	SB1	yes
α Ser	140573	K2III	2.64	0.84	...	~0	S	no
δ CrB	141714	G3.5IV-III	4.63	0.65	45.	<15	S	yes
MS Ser	143313	K2V/K6V	8.36	0.74/	9.60	...	SB2	yes
σ^2 CrB	146361	F6V/G0V	5.7	0.50	1.168	26/25	SB2	yes
HR 6469	157482	[ ]/G5IV	5.51	[ ]/0.61	81.9	[ ]/6	SB3	yes
29 Dra	160538	WD/K0-2III	6.55	/0.77	28.8	/8	SB1	yes
β Oph	161096	K2III	2.77	0.84	[470]	1.6	S	no
μ Her(A)	161797	G5IV	3.42	0.61	[100]	1.1	S	no
HR 6806	166469	K2V	6.40	0.74	[13]	2.5[b]	S	no
V775 Her	175742	K0V	8.04	0.64	2.898	15	SB1	yes
HR 7275	179094	K1IV-III	5.81	0.80	28.	15	SB1	yes
V1764 Cyg	185151	K1III	7.69	0.81	40.25	28	SB1	yes
β Aql	188512	G8IV	3.71	0.64	[50]	2.2	S	no
BD+15°4057	191262	G5V/G5V	7.79	0.54/0.54	orb5.43	6/6	SB2	yes
61 Cyg A	201091	K5V	5.23	0.99	37.9	~0	S	no
61 Cyg B	201092	K7V	6.03	1.15	48.	4[b]	S	no
HR 8703	216489	K2III-II	5.60	0.84	24.39	24	SB1	yes
λ And	222107	G8IV-III	3.7	0.70	53.952	10	SB1	yes
HR 9024	223460	G1III	5.90	0.54	22.61	20	S	yes
II Peg	224085	K1IV	7.2	0.81	6.718	21	SB1	yes
SUN	...	G2V	...	0.53	25.38	2	S	no

[a]A period in brackets is an estimate from $v \sin i$.
[b]New measure this paper.
[c]From the spectral type–color relation of Johnson 1966.
[d]Close visual binary.

TABLE 3

BALMER Hε AND Ca II H AND K ABSOLUTE EMISSION-LINE FLUXES

Star Name	T_{eff} (K)	log $\mathcal{F}$(Hε)	log $\mathcal{F}$(K_1)	log $\mathcal{F}$(H_1) (erg $cm^{-2}s^{-1}$)	log $\mathcal{F}$'(K_1)	log $\mathcal{F}$'(H_1)	R_{HK}[a] (–)	Code
δ And	4200	...	5.42	5.23	5.39	5.20	2.3(-5)	KPNO0.24
		...	5.42	5.22	5.39	5.20	2.3(-5)	KPNO0.24
		...	5.40	5.22	5.37	5.19	2.2(-5)	KPNO0.24
		...	5.38	5.20	5.36	5.17	2.1(-5)	KPNO0.24
AY Cet	5150	...	6.55	6.41	6.54	6.40	1.5(-4)	KPNO0.24
HR 339	5850	...	6.48	6.56	6.43	6.53	9.2(-5)	DAORET0.5
HR 454	4600	...	6.61	6.38	6.61	6.38	2.5(-4)	KPNO0.24
		...	6.41	6.42	6.40	6.41	2.0(-4)	DAORET0.5
		...	6.45	6.44	6.44	6.43	2.2(-4)	DAORET0.5
		...	6.44	6.48	6.43	6.48	2.3(-4)	DAORET0.5
HD 12545	4750	...	6.72	6.67	6.72	6.67	3.4(-4)	DAORET0.5
		...	6.66	6.63	6.66	6.63	3.0(-4)	DAORET0.5
HD 17433	4400	...	6.15	6.15	6.14	6.14	5.7(-5)	DAORET0.5
HD 19485c[b]	5700	...	6.74	6.67	6.72	6.65	1.6(-4)	KPNO0.24
HD 19485h[b]	5800	...	6.64	6.56	6.61	6.53	1.2(-4)	KPNO0.24
HR 1023	5150	...	6.29	6.25	6.28	6.23	9.0(-5)	KPNO0.24
UX Ari[c]	/5000	...	6.34	6.37	6.26	6.31	1.1(-4)	DAORET0.5
V711 Tau[c]	/4840	...	6.44	6.44	6.43	6.43	1.7(-4)	DAORET0.5
10 Tau	6115	...	5.86	5.81	5.26	5.35	5.1(-6)	KPNO0.30
HR 1176[d]	/5450	...	6.25	6.17	6.22	6.14	6.1(-5)	KPNO0.24
V491 Per A[d]	5235	...	6.38	6.26	6.36	6.24	9.4(-5)	KPNO0.30
EI Eri	5460	...	6.80	6.70	6.79	6.69	2.2(-4)	KPNO0.24
		...	6.80	6.70	6.79	6.69	2.2(-4)	KPNO0.24
		...	6.54	6.58	6.52	6.58	1.4(-4)	DAORET0.5
		...	6.72	6.66	6.71	6.66	1.9(-4)	DAORET0.5
HR 1362	5235	...	6.54	6.42	6.52	6.40	1.4(-4)	KPNO0.24
HD 27691	6030	...	6.48	6.36	6.41	6.27	6.0(-5)	KPNO0.24
V492 Per	4600	...	6.20	6.04	6.20	6.02	1.0(-4)	KPNO0.24
HR 1455[d]	5100	...	4.79[e]	4.67[e]	...	...	...	KPNO0.24
		...	4.89[e]	4.80[e]	...	...	...	KPNO0.30
BD+26°730	4350	...	6.00	6.08	5.99	6.07	1.1(-4)	DAOCCD0.9
HD 30957[d]	5235	...	6.59	6.43	6.57	6.41	1.5(-4)	KPNO0.24
HD 31738[d]	5460	(6.27:)	6.81	6.72	6.80	6.71	2.3(-4)	KPNO0.24
		...	6.70	6.68	6.69	6.67	1.9(-4)	DAORET0.5
HD 31993	4420	...	6.23	6.13	6.22	6.12	1.4(-4)	KPNO0.30
12 Cam	4750	...	6.41	6.37	6.40	6.36	1.7(-4)	DAOCCD0.9
HD 33798	4750	...	6.34	6.16	6.33	6.15	1.2(-4)	KPNO0.24
HD 34198	4750	...	6.37	6.21	6.36	6.20	1.3(-4)	KPNO0.24
HR 1908	4000	...	5.03	4.97	4.96	4.90	1.2(-5)	DAOCCD0.9
χ^1 Ori	6030	...	6.54	6.57	6.48	6.52	8.4(-5)	DAORET0.5
		...	6.54	6.47	6.48	6.41	7.4(-5)	DAORET0.5
		...	6.67	6.58	6.62	6.53	1.0(-4)	DAOCCD0.9
		...	6.64	6.57	6.59	6.52	9.6(-5)	DAOCCD0.9
HR 2081	5150	...	<5.4[f]	<5.4[f]	...	...	...	DAOCCD0.9
1 Gem[d]	/4750	...	5.37	5.29	5.28	5.18	1.2(-5)	KPNO0.30
OU Gem[c]	4730/	...	6.15	6.18	6.13	6.17	1.0(-4)	DAORET0.5
		...	6.17	6.16	6.16	6.15	1.0(-4)	DAOCCD0.9
σ Gem	4600	...	6.20	6.04	6.19	6.02	1.0(-4)	KPNO0.30
		...	6.22	6.21	6.21	6.20	1.3(-4)	DAORET0.5
		...	6.25	6.24	6.24	6.23	1.4(-4)	DAORET0.5
		...	6.26	6.20	6.25	6.19	1.3(-4)	DAOCCD0.9
		...	6.27	6.21	6.26	6.20	1.4(-4)	DAOCCD0.9
κ Gem	4900	...	5.38	5.34	5.25	5.21	1.0(-5)	KPNO0.30
β Gem	4750	...	5.36	5.22	5.27	5.11	9.5(-6)	KPNO0.24
		...	5.30	5.19	5.20	5.10	9.5(-6)	KPNO0.24
		...	5.29	5.21	5.18	5.10	9.5(-6)	KPNO0.30
HD 65195[d]	5150	...	6.08	6.04	6.06	6.01	5.4(-5)	KPNO0.24
		...	6.25	6.24	6.23	6.22	8.5(-5)	DAOCCD0.9
54 Cam[d]	6060	...	6.70	6.59	6.66	6.55	1.1(-4)	KPNO0.30
		...	6.62	6.58	6.58	6.54	9.6(-5)	DAORET0.5
		...	6.69	6.67	6.66	6.64	1.2(-4)	DAOCCD0.9
28 Mon	4000	...	4.88	5.01	4.78	4.95	1.0(-5)	DAORET0.5
o UMa	5150	...	5.55	5.44	5.45	5.33	1.2(-5)	KPNO0.30
35 Cnc[g]	5850	...	...	...	...	...	...	DAORET0.5
		...	...	...	...	...	...	DAOCCD0.9
π^1 UMa	6030	...	6.57	6.46	6.51	6.39	7.6(-5)	KPNO0.30
Gliese 338 A	3850	...	4.86	4.83	4.84	4.81	1.1(-5)	DAOCCD0.9
		...	4.90	4.83	4.88	4.81	1.1(-5)	DAOCCD0.9
HD 80715a[b]	4730	(5.79)	6.45	6.28	6.45	6.28	1.6(-4)	KPNO0.24
HD 80715b[b]	4730	5.79	6.45	6.32	6.45	6.31	1.7(-4)	KPNO0.24
IL Hya	4600	5.66	6.36	6.29	6.35	6.28	1.6(-4)	KPNO0.30

TABLE 3—*Continued*

Star Name	T_{eff} (K)	log $\mathcal{F}$(Hϵ)	log $\mathcal{F}(K_1)$	log $\mathcal{F}(H_1)$ ($erg\ cm^{-2}s^{-1}$)	log $\mathcal{F}'(K_1)$	log $\mathcal{F}'(H_1)$	R_{HK}[a] (–)	Code
24 UMa	5200	...	6.16	6.15	6.14	6.13	6.6(-5)	DAORET0.5
		...	6.33	6.28	6.32	6.27	9.4(-5)	DAOCCD0.9
		...	6.22	6.21	6.20	6.19	7.6(-5)	DAOCCD0.9
		...	6.20	6.17	6.18	6.15	7.1(-5)	DAOCCD0.5
LQ Hya	5250	6.68	7.05	6.89	7.04	6.88	4.3(-4)	KPNO0.24
Gliese 378.1	4000	4.49	5.09	4.88	5.07	4.85	1.3(-5)	KPNO0.24
		...	5.03	4.97	5.01	4.95	1.3(-5)	DAOCCD0.9
Gliese 380	4060	...	5.08	5.11	5.06	5.09	1.6(-5)	DAORET0.5
		...	5.24	5.18	5.23	5.17	2.0(-5)	DAOCCD0.9
		...	5.28	5.24	5.27	5.23	2.3(-5)	DAOCCD0.9
LR Hya[c]	5250	...	6.41	6.34	6.38	6.31	1.0(-4)	KPNO0.30
Gliese 410	3580	...	4.88	4.89	4.88	4.89	1.6(-5)	DAOCCD0.9
ξ UMa(B)	5770	...	6.31	6.18	6.24	6.11	4.8(-5)	KPNO0.24
HR 4430	4420	...	5.86	5.73	5.85	5.71	5.6(-5)	KPNO0.24
		...	5.70	5.57	5.68	5.54	3.8(-5)	DAOCCD0.9
		...	5.64	5.55	5.61	5.52	3.4(-5)	DAOCCD0.5
DF UMa[c]	3850	...	5.14	5.24	5.13	5.23	2.5(-5)	DAOCCD0.9
61 UMa	5570	...	6.18	6.09	5.99	5.91	3.3(-5)	KPNO0.30
		...	6.29	6.33	6.24	6.29	6.7(-5)	DAORET0.5
		...	6.37	6.29	6.33	6.24	7.1(-5)	DAOCCD0.9
		...	6.30	6.29	6.25	6.24	6.5(-5)	DAOCCD0.5
β Vir	6115	...	5.91	5.87	5.43	5.51	7.5(-6)	KPNO0.30
HD 106225	4750	6.09	6.70	6.61	6.69	6.60	3.1(-4)	KPNO0.30
		...	6.59	6.64	6.58	6.64	2.8(-4)	DAOCCD0.9
31 Com	5850	...	6.67	6.65	6.64	6.62	1.3(-4)	DAORET0.5
		...	...	...	...	...	...	DAOCCD0.9
HD 113983	4900	...	5.48	5.37	5.38	5.25	1.3(-5)	KPNO0.30
HD 115781[d]	4750	...	6.50	6.32	6.49	6.31	1.8(-4)	KPNO0.24
		...	6.39	6.35	6.38	6.34	1.6(-4)	DAOCCD0.9
		...	6.33	6.21	6.32	6.20	1.3(-4)	DAOCCD0.5
HD 116204	4600	...	6.51	6.46	6.50	6.45	2.4(-4)	DAOCCD0.9
		...	6.46	6.46	6.45	6.45	2.2(-4)	DAOCCD0.9
		...	6.48	6.46	6.47	6.45	2.3(-4)	DAOCCD0.9
		...	6.44	6.35	6.43	6.34	1.9(-4)	DAOCCD0.5
HD 116378	5770	...	6.38	6.33	6.32	6.28	6.3(-5)	DAOCCD0.9
70 Vir	5800	...	5.77	5.73	5.44	5.46	8.7(-6)	KPNO0.30
FK Com	5450	...	7.32	7.18	7.32	7.18	7.2(-4)	DAOCCD0.9
HR 5110[d]	/4660	...	5.72	5.82	5.68	5.80	4.2(-5)	KPNO0.24
		...	...	...	...	...	...	DAOCCD0.9
		...	...	...	...	...	...	DAOCCD0.9
		...	5.64	5.52	5.59	5.47	2.6(-5)	DAOCCD0.5
η Boo	5940	...	5.83	5.75	5.51	5.42	8.3(-6)	KPNO0.30
4 UMi	4200	...	5.32	5.15	5.29	5.11	1.8(-5)	KPNO0.24
HR 5534	6030	...	6.46	6.48	6.38	6.42	6.7(-5)	DAOCCD0.5
ξ Boo A	5570	...	6.65	6.60	6.63	6.58	1.5(-4)	DAOCCD0.9
		...	6.65	6.60	6.63	6.58	1.5(-4)	DAOCCD0.9
		...	6.48	6.44	6.45	6.41	9.8(-5)	DAOCCD0.5
ξ Boo B	4590	...	5.88	5.84	5.86	5.82	5.6(-5)	DAOCCD0.9
		...	5.86	5.79	5.84	5.77	5.1(-5)	DAOCCD0.5
HR 5553	4900	...	6.15	6.08	6.13	6.06	7.6(-5)	DAOCCD0.9
		...	6.13	6.02	6.11	5.99	6.9(-5)	DAOCCD0.9
		...	6.15	6.12	6.13	6.10	7.9(-5)	DAOCCD0.9
		...	6.15	6.10	6.13	6.08	7.6(-5)	DAOCCD0.9
		...	5.96	5.94	5.92	5.91	5.0(-5)	DAOCCD0.5
UV CrB	4600	...	6.20	6.14	6.19	6.13	1.1(-4)	KPNO0.30
δ CrB	5300	...	6.15	6.12	6.12	6.10	5.8(-5)	DAOCCD0.9
		...	6.20	6.11	6.18	6.08	6.1(-5)	DAOCCD0.9
		...	6.08	6.05	6.05	6.02	4.8(-5)	DAOCCD0.5
HD 143313[c]	4900/	...	6.58	6.54	6.57	6.53	2.2(-4)	DAOCCD0.9
σ^2 CrB[c]	/6030	...	7.08	6.97	7.06	6.95	2.7(-4)	DAOCCD0.9
		...	6.93	6.91	6.91	6.89	2.1(-4)	DAOCCD0.5
HR 6469[d]	5460	...	6.12	6.09	6.09	6.05	4.7(-5)	DAOCCD0.5
29 Dra	4600	...	6.41	6.35	6.40	6.34	1.9(-4)	DAOCCD0.5
μ Her	5460	...	5.52	5.44	5.23	5.14	6.1(-6)	KPNO0.30
HD 175742	5250	6.48	6.71	6.67	6.70	6.66	2.2(-4)	DAOCCD0.5
V1764 Cyg	4600	...	6.33	6.24	6.33	6.23	1.5(-4)	KPNO0.30
HD 191262a[b]	5770	...	6.47	6.45	6.42	6.41	8.3(-5)	KPNO0.30
HD 191262b[b]	5770	...	6.54	6.46	6.50	6.42	9.3(-5)	KPNO0.30
HR 8703	4420	...	6.36	6.41	6.35	6.41	2.2(-4)	DAORET0.5
λ And	4900	...	6.46	6.46	6.45	6.45	1.7(-4)	DAORET0.5
		...	6.49	6.49	6.48	6.48	1.8(-4)	DAORET0.5
		...	6.50	6.47	6.49	6.46	1.8(-4)	DAORET0.5
HR 9024	5650	...	6.74	6.72	6.73	6.71	1.8(-4)	DAORET0.5
II Peg	4840	...	6.47	6.47	6.46	6.46	1.9(-4)	DAORET0.5
SUN (Sky)	5860	...	5.85	5.72	5.72	5.56	1.3(-5)	KPNO0.30

[a] The value in parentheses is the power of 10.

[b] Both components show H and K emission. The given fluxes have been corrected for the presence of two continua (see Table 2).

[c] Both components show H and K emission. The given fluxes are the combined fluxes from both components.

[d] Fluxes are contaminated by the continuum of the (presumably hotter) secondary component.

[e] This measure is approximately our lower limit for reliable fluxes from the 0.24 Å KPNO data.

[f] This measure is approximately our lower limit for reliable fluxes from the 0.9 Å DAO data.

[g] H and K emission too weak to measure (see Fig. 10).

TABLE 4

BALMER Hε AND Ca II H AND K MEAN EQUIVALENT WIDTHS AND LINE WIDTHS FOR THE 0.24 AND 0.30 Å RESOLUTION KPNO DATA

Star Name	W(Hε) (Å)	W(K) (Å)	W(H) (Å)	W_0(K) (Å)	W_0(H) (Å)	$\Delta\lambda_{(K_1)}$ (Å)	$\Delta\lambda_{(H_1)}$ (Å)	$\Delta\lambda_{(K_2)}$ (Å)	$\Delta\lambda_{(H_2)}$ (Å)	FWHM(K) (Å)	FWHM(H) (Å)
δ And	...	0.148	0.066	0.239	0.157	1.57	1.40	0.66	0.61	0.70	0.79
AY Cet	...	0.711	0.475	1.001	0.723	1.92	1.57	...	...	0.70	0.65
HR 454	...	2.020	1.130	2.143	1.262	2.79	1.92	...	...	1.13	0.96
HD 19485c[b]	...	0.320	0.258	0.559	0.474	1.27	1.40	...	...	0.59	0.57
HD 19485h[b]	...	0.200	0.160	0.475	0.396	blend	1.22:	...	...	0.49:	0.78:
HR 1023	...	0.164	0.105	0.558	0.503	2.44	2.70	1.04	1.66	...	...
10 Tau	...	...	...	0.057	0.050	...	...	...	...	...	...
HR 1176[a]	...	0.063	0.063	0.336	0.280	1.48	1.40	0.52	0.52	0.84	0.79
V491 Per A[a]	...	0.363	0.252	0.453	0.346	1.05	1.31	...	...	0.52	0.49
V491 Per B[a]	...	0.060:	0.040:	0.240	0.182	blend	0.62	...	...	blend	0.26
EI Eri	...	0.620	0.352	1.303	1.041	2.42	2.27	...	...	0.87	0.96
HR 1362	...	0.418	0.283	0.580	0.443	1.57	1.48	0.44	0.40	0.84	0.77
HD 27691	...	0.058	0.040	0.300	0.225	...	...	...	...	...	...
V492 Per	...	0.630	0.360	0.972	0.658	2.10	1.92	...	...	1.05	0.96
HR 1455[a]	...	...	...	0.025	0.019	...	...	...	...	...	...
HD 30957[a]	...	0.468	0.301	0.827	0.580	1.40	1.26	...	...	0.73	0.84
HD 31738[a]	0.052:	0.781	0.463	1.235	0.997	2.10	1.92	...	...	0.52	0.47
HD 31993	...	0.816	0.551	1.323	1.053	2.95	2.32	0.54	...	1.50	1.16
HD 33798	...	0.698	0.410	1.098	0.727	1.40	1.92	...	...	1.00	0.84
HD 34198	...	0.635	0.368	1.020	0.702	1.43	1.91	0.70:	0.52	1.34	1.19
1 Gem[a]	...	0.096	0.041	0.142	0.115	0.62:	0.77:	...	...	0.46:	0.62:
σ Gem	...	0.835	0.506	1.026	0.696	2.20	1.82	...	...	0.95	0.89
κ Gem	...	0.023	0.021	0.064	0.058	1.07	1.18	0.62	0.64	0.48	...
β Gem	...	0.038	0.024	0.090	0.065	1.13	1.05	0.56	0.61	0.53	0.78:
HD 65195[a]	...	0.207	0.150	0.380	0.340	1.22	1.24	...	...	0.65	0.70
54 Cam[a]	...	0.133	0.090	0.456	0.356	1.55	1.24	...	...	0.67	0.62
o UMa	...	0.042	0.039	0.090	0.070	1.27	1.00	0.73	0.68	...	...
π^1 UMa	...	0.183	0.142	0.328	0.255	1.09	0.92	0.14	...	0.54	0.49
HD 80715a[b]	blend	1.742	1.076	2.028	1.374	blend	blend	...	...	0.40	0.35
HD 80715b[b]	0.094	1.758	1.116	2.027	1.489	blend	blend	...	...	0.49	0.35
IL Hya	0.025	1.328	1.011	1.722	1.478	2.48	2.01	...	...	0.82	0.70
LQ Hya	0.306	1.480	0.933	1.853	1.284	1.40	1.40	...	...	0.48	0.44
Gl 378.1	0.055	0.978	0.576	1.182	0.727	0.87	0.77	...	...	0.42	0.38
LR Hya[c]	...	0.316	0.237	0.498	0.423	1.24	1.28	...	...	0.59	0.54
ξ UMa B	...	0.082	0.074	0.253	0.187	1.05	0.87	...	...	0.38	0.35
HR 4430	...	0.282	0.159	0.461	0.337	1.75	1.75	0.58	0.49	1.19	1.05
61 UMa	...	0.107	0.088	0.213	0.174	0.91	0.80	0.21	0.20	0.54	0.51
β Vir	...	...	...	0.060	0.060:	0.93:	0.77:	...	...	...	...
HD 106225	0.182	2.244	1.620	2.682	2.185	2.63	2.17	...	...	0.85	0.73
HD 113983	...	0.043	0.025	0.122	0.094	1.05	...	0.57	...	0.57	...
HD 115781[a]	...	1.020	0.572	1.673	1.104	2.79	2.44	...	...	1.13	0.96
70 Vir	...	0.21	0.21	0.061	0.056	0.71	0.70:	0.55	0.56:	...	...
HR 5110[a]	...	0.179	0.369	0.485	0.614	1.08	0.96	...	...	0.47	0.40
η Boo	...	...	...	0.056	0.047	0.75:	0.60:	...	...	...	...
4 UMi	...	0.160	0.080	0.261	0.176	1.57	1.48	0.80	0.70	1.22	0.84
UV CrB	...	0.620	0.447	1.080	0.946	2.79	2.63	...	...	1.33	1.15
μ Her	...	...	...	0.059	0.050	0.77:	0.74:	0.46	...	0.38	...
V1764 Cyg	...	0.910	0.679	1.586	1.278	3.10	2.94	0.65	0.47	1.70	1.49
HD 191262a[b]	...	0.142	0.140	0.306	0.297	0.93:	1.95:	...	...	0.54	0.50
HD 191262b[b]	...	0.184	0.154	0.365	0.301	0.93:	1.08:	0.19	0.14	0.54	0.57
SUN (Sky)	...	0.009	...	0.080	0.060	0.77	...	0.46	...	0.31	...

[a]Equivalent widths are contaminated by an unknown amount of continuum of the secondary component. No correction has been applied.

[b]Ca II H and K emission from both components resolved. We assumed equal continua due to the nearly identical absorption line strengths and multiplied the measured equivalent widths by a factor of 2.

[c]Both components show H and K emission but the lines are blended in our spectra. Due to the similarity of the spectral types, however, no corrections for continuum are necessary.

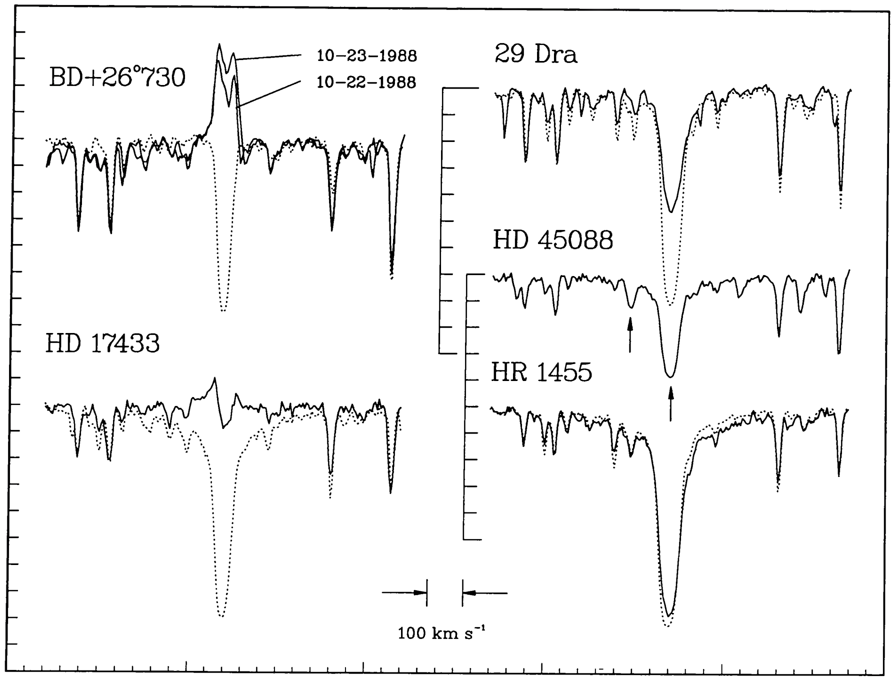

FIG. 4.—Hα profiles for five program stars. Each of the five stars represents a typical example of a particular type of Hα line profile. The dotted lines are spectra of reference stars of the same spectral type and luminosity class. All spectra are on the same scale but are shifted in intensity for better display. *BD + 26°730:* Strong and variable emission line. The spectra from two consecutive nights (phase difference ≈ 0.5) have been shifted in wavelength to align their respective photospheric absorption features. *HD 17433:* Weak emission line with strong superposed absorption profile. *29 Dra:* Filled-in absorption-line profile. *HD 45088:* Filled-in absorption-line profiles in a double-lined spectroscopic binary (the arrows indicate the two Hα lines). *HR 1455:* Composite Hα absorption profile. The deep core is primarily from the G5 III primary while the wings are dominated by an early F star.

stars which have σ_W less than 60 mÅ, and Table 6B gives the individual observations for the stars with variable Hα line profile, i.e., if σ_W is greater than 60 mÅ.

In the following part we will briefly describe the spectroscopic features of the not-so-well known and/or very peculiar program stars but do not intend to give a full discussion of all the individual stars. For references on most of the active *binary* stars in this paper see the "Chromospherically Active Binary Star" (= CABS) catalog (Strassmeier *et al.* 1988) and also the discussion in Fekel, Moffett, and Henry (1986).

HD 7672.—Strong Ca II H and K emission at a flux level of log $\mathscr{F}$(K) ~ 6.55 ergs cm^{-2} s^{-1}. Hα is an absorption feature clearly filled in by emission.

HR 339 = ψ^3 *Psc.*—Approximately the same Ca II H and K flux level as HD 7672 but no obvious emission features are visible (Fig. 10). Our one Hα spectrum shows a strong absorption profile, but no appropriate reference star spectrum was available for this early G giant.

HD 9746.—Broad Ca II H and K emission lines with equivalent widths of +2 Å and +1.1 Å for the K and H line, respectively (Table 4). The Hα absorption line is very shallow and has a blueshifted emission feature of about 30 ± 5 mÅ.

HD 12545.—This is one of the few systems with Hα consistently in emission. Its equivalent width is highly variable (Table 6B) and in strength comparable to V711 Tau. Hε seems to be also an emission feature. The two Ca II H and K spectra show strong emission features above the continuum and may also indicate moderate variability of the K line (Table 3).

HD 17433.—Strong Ca II H and K emission features with emission-line flux of log $\mathscr{F}$(K) ~ 6.15—*if* the star is a subgiant rather than a G9 dwarf as previously thought (otherwise our measurement of the line flux would be ≈ 6.80 if $V-R$ = 0.64). The Hα line profile consists of an emission feature with a strong and broad central reversal (Fig. 4). The equivalent width and residual intensity listed in Table 6A are estimates. Recently, Bopp *et al.* (1989) found the Hα line varying from a pure emission profile to an absorption profile with occasionally enhanced Hα emission presumably related to flare events.

HD 19485.—This double-lined spectroscopic binary shows double H and K emission (Fig. 10) at an emission-line flux level of log $\mathscr{F}$(K) ~ 6.7 and 6.6 for the G6 and G4 component, respectively. Hα is a double absorption feature with the weaker line belonging to the cooler (presumably more active) component.

HR 1023.—The H and K line profiles show H_2 and K_2 points at a flux level of log $\mathscr{F}$(K) ~ 6.3. The strong central reversal obscures the emission line, and high resolution is needed to resolve the H_1 and K_1 points. Hα is a very strong absorption line with an equivalent width 440 mÅ larger than the reference star o UMa.

UX Ari.—Hε in emission.

TABLE 5

BALMER Hα REFERENCE STARS

Star Name	Spectral Type[a]	$\langle W_\alpha \rangle$ (Å)	σ_W (Å)	$\langle R_c \rangle$	σ_{R_c}	n	Observatory Code
			Dwarfs				
β Vir	F9 V	−1.240	0.000	0.191	0.000	2	KNO0.18
		−1.367	0.040	0.232	0.004	4	2.1McD0.28
β Com......	G0 V	−1.570	0.017	0.261	0.006	3	Ritter0.3
70 Vir	G4 V	−1.059	0.003	0.174	0.005	2	KPNO0.18
HR 166	K0 V	−0.947	...	0.205	...	1	KPNO0.18
HR 6806 ...	K2 V	−0.877	0.020	0.205	0.004	2	KPNO0.18
61 Cyg A ...	K5 V	−0.678	0.009	0.395	0.003	2	Ritter0.3
61 Cyg B ...	K7 V	−0.565	...	0.347	...	1	KPNO0.18
10 Tau......	F9 IV–V	−1.155	...	0.175	...	1	KPNO0.21
			Subgiants				
τ Boo.......	F6 IV	−1.909	0.065	0.278	0.002	2	Ritter0.3
η Boo.......	G0 IV	−1.262	0.006	0.187	0.000	2	KPNO0.18
		−1.675	0.050	0.228	0.003	2	Ritter0.3
μ Her.......	G5 IV	−1.056	0.003	0.181	0.000	2	KPNO0.18
		−1.078	0.025	0.239	0.011	4	2.1McD0.28
		−1.260	0.020	0.251	0.007	5	Ritter0.3
β Aql.......	G8 IV	−1.002	0.001	0.182	0.000	2	KPNO0.18
δ Eri	K0 IV	−1.019	...	0.290	...	1	2.1McD0.42
			Giants				
o UMa......	G5 III	−1.179	0.010	0.176	0.000	2	KPNO0.18
κ Gem......	G8 III	−1.077	0.003	0.176	0.002	2	KPNO0.18
ε Vir	G8 III	−1.280	...	0.251	...	2	Ritter0.3
ε Boo	K0 II–III	−1.258	0.004	0.244	0.004	2	Ritter0.3
β Gem......	K0 III	−1.052	0.002	0.183	0.003	2	KPNO0.18
		−1.019	0.009	0.243	0.003	11	2.1McD0.28
		−1.039	...	0.205	...	1	KPNO0.4
		−1.137	0.019	0.249	0.005	38	Ritter0.3
α Boo.......	K1 III	−1.130	0.016	0.253	0.002	7	2.1McD0.42
		−1.109	...	0.225	...	1	2.7McD0.35
		−1.148	...	0.204	...	1	KPNO0.4
		−1.260	0.027	0.219	0.007	24	Ritter0.3
α Ari	K2 III	−1.033	0.004	0.266	0.006	9	2.1McD0.42
β Oph......	K2 III	−0.999	0.010	0.193	0.002	3	KPNO0.18
		−1.015	...	0.270	...	1	2.1McD0.42
		−0.976	0.034	0.289	0.011	12	Ritter0.3
α Ser	K2 III	−1.007	0.009	0.275	0.005	3	Ritter0.3
ρ Boo.......	K3 III	−1.082	0.052	0.256	0.006	5	Ritter0.3
β Cnc	K4 III	−1.091	0.005	0.224	0.011	2	Ritter0.3

[a] Taken from Keenan 1983.

V711 Tau.—Hε in emission.

HR 1176.—Our only Ca II spectrum shows weak blueshifted H and K emission lines with large V/R emission ratio. Hα appears to be a normal absorption feature.

HD 25893.—The star is a close visual binary, V491 Per A (= the G8 IV primary) and B, with strong emission from the A component and weak emission from the B component. Observations in the red at 6430 Å show only lines from the G8 IV component. Hα is a filled-in absorption line.

HD 26337.—The Ca II K line flux might be variable.

HR 1362.—This single star has the longest known rotation period for a chromospherically active star (310 days; Strassmeier and Hall 1988) and high Ca II emission-line flux of log $\mathcal{F}$(K) ~ 6.5. Both emission lines show reversals. Hα appears to be a rather normal absorption line.

HD 27691.—Although no obvious H and K emission lines are visible (Fig. 10), the flux level of this G0 dwarf is nevertheless quite high, log $\mathcal{F}$(K) ~ 6.5. However, Hα is a rather strong absorption feature, stronger than that in the reference star β Vir.

HR 1455.—This star is one of the few examples in the candidate list of the CABS catalog where we could not detect chromospheric H and K emission. Our 0.21 Å CCD spectrum of the Hα region shows a composite Hα line profile of an

TABLE 6A

BALMER Hα EQUIVALENT WIDTHS AND RESIDUAL INTENSITIES

Star Name	$<W_\alpha>$ (Å)	σ_W (Å)	$<R_c>$	σ_{R_c}	$<W_{em}>$ (Å)	n	Reference Star	Observatory Code
This paper								
δ And	-0.982	...	0.201	...	+0.025	1	β Oph	KPNO0.18
AY Cet	-0.805	0.019	0.517	0.006	+0.374	2	o UMa	2.1McD0.42
HR 339	-2.185	...	0.444	...	...	1	...	KPNO0.2
HR 454	-0.615	0.007	0.622	0.009	+0.494	3	α Boo	2.1McD0.42
HD 17433	~0.0	...	~1.0	...	+0.947	1	HR 166	KPNO0.21
HD 19485(h)	-1.508[a]	...	0.457	...	-0.420:	1	70 Vir	KPNO0.18
HD 19485(c)	-1.005[a]	...	0.645	...	+0.054:	1	70 Vir	KPNO0.18
HR 1023	-1.650	0.010	0.331	0.002	-0.437	2	o UMa	2.1McD0.42
UX Ari	+0.091	...	1.100	...	+1.205	1	δ Eri	KPNO0.2
HR 1176	-1.207	...	0.336	...	-0.028	1	o UMa	2.1McD0.42
V491 Per[b]	-0.865	...	0.427	...	+0.146	1	β Aql	2.1McD0.42
HR 1362	-1.044	0.013	0.308	0.023	-0.042	2	β Aql	2.1McD0.28
HD 27691	-1.484	...	0.334	...	-0.100	1	β Vir	2.1McD0.42
V492 Per	-1.140	...	0.430	...	+0.020	1	α Boo	2.1McD0.28
HR 1455[b]	-1.130	...	0.219	...	+0.049	1	o UMa	KPNO0.21
HD 30957[b]	-0.909	...	0.589	...	+0.093	1	β Aql	2.1McD0.28
HD 31738[b]	-0.403	...	0.766	...	+0.703	1	μ Her	2.1McD0.28
HD 31993	-1.386	...	0.424	...	-0.324	1	β Oph	2.1McD0.28
HD 33798	-1.081	...	0.446	...	+0.025	1	β Gem	2.1McD0.28
HD 34198	-1.205	...	0.433	...	-0.144	1	β Gem	2.1McD0.28
HR 1908	-1.030	0.010	0.227	0.003	+0.061	2	β Cnc	Ritter0.3
χ^1 Ori	-1.617	0.041	0.332	0.011	-0.047	6	β Com	Ritter0.3
HR 2081[b]	-1.645	0.036	0.369	0.045	-0.438	4	o UMa	Ritter0.3
1 Gem[b]	-1.072	...	0.216	...	-0.020	1	β Gem	KPNO0.21
HD 45088(h)	-0.663[d]	...	0.611	...	+0.214	1	HR 6806	KPNO0.21
HD 45088(c)	-0.253[d]	...	0.871	...	+0.312	1	61 Cyg B	KPNO0.21
HD 65195	-1.130	...	0.372	...	+0.049	1	o UMa	KPNO0.4
54 Cam[b]	-1.127	...	0.442	...	+0.135	1	η Boo	2.1McD0.28
28 Mon	-1.148	0.026	0.237	0.012	-0.057	6	β Cnc	Ritter0.3
Gliese 378.1	-0.678	...	0.432	...	-0.100	1	61 Cyg B	KPNO0.4
Gliese 380	-0.608	0.004	0.399	0.011	-0.043	4	61 Cyg B	KPNO0.4;0.5
LR Hya a	-0.890[d]	...	0.649	...	+0.057	1	HR 166	2.1McD0.28
LR Hya b	-1.038[d]	...	0.657	...	-0.091	1	HR 166	2.1McD0.28
ξ UMa B	-0.962	...	0.473	...	+0.097	1	70 Vir	KPNO0.4
HR 4430	-1.259	0.059	0.321	0.018	-0.259	10	β Oph	Ritter0.3
DF UMa[b]	+1.153	...	1.35	...	+1.718	1	61 Cyg B	KPNO0.5
61 UMa	-1.136	0.048	0.265	0.004	-0.158	6	HR 166	KPNO0.4;0.5
HD 113983	-1.005	...	0.278	...	+0.072	1	κ Gem	2.1McD0.28
HD 115781[b]	-1.100	0.009	0.561	0.071	+0.020	4	β Gem	2.1McD0.28
HD 116204	-0.649	0.047	0.590	0.018	+0.381	4	β Gem	2.1McD0.42
HD 116378	-1.079	...	0.280	...	-0.020	1	70 Vir	2.1McD0.42
4 UMi	-1.145	...	0.170	...	-0.138	1	β Oph	KPNO0.18
HR 5534	-1.466	0.017	0.322	0.013	+0.104	6	β Com	Ritter0.3
ξ Boo A	-1.193	0.060	0.404	0.024	-0.247:	8	HR 166	Ritter0.3
ξ Boo B	-0.654	...	0.519	...	+0.024	1	61 Cyg A	Ritter0.3
HR 5553	-0.987	...	0.355	...	-0.090	1	HR 6806	2.1McD0.25
	-1.015	0.067[c]	0.386	0.030	-0.138:	13	HR 6806	Ritter0.3
UV CrB	-1.213	...	0.437	...	-0.023	1	β Oph	2.1McD0.42
V775 Her	-0.161	...	0.825	...	+0.736	1	HR 6806	2.7McD0.35
V1764 Cyg	-1.216	0.058	0.482	0.080	-0.020	2	α Boo	2.1McD0.42
HR 9024	-1.241	0.050	0.464	0.005	-0.028	3	o UMa	2.1McD0.42
Bopp, Dempsey, and Maniak (1988)								
σ Gem	-1.099	0.075	0.445	0.027	+0.038	56	β Gem	Ritter0.3
35 Cnc	-2.397	0.215	0.417	0.030	...	9	...	Ritter0.3
24 UMa	-1.264	0.032	0.336	0.024	-0.004	25	μ Her	Ritter0.3
31 Com	-2.088	0.135	0.436	0.035	...	21	...	Ritter0.3
δ CrB	-1.288	0.051	0.319	0.016	-0.028	15	μ Her	Ritter0.3
λ And	-0.920	0.050	0.476	0.023	+0.360	34	ϵ Vir	Ritter0.3
Barden and Nations (1988)								
HD 80715 a	...	...	...	...	+0.421	12	...	KPNO CF
HD 80715 b	...	...	...	...	+0.544	12	...	KPNO CF
Walter and Basri (1982)								
FK Com	<+3.3>	~2.0	...	...	...	95	...	Lick
Strassmeier, Weichinger, and Hanslmeier (1986)								
HR 5110[b]	-0.715	0.065	0.760	0.010	...	2	...	Vienna

[a] Corrected for the presence of two continua. Although the Hα cores are well separated, both Hα lines show pronounced wings which are strongly blended, and the measured equivalent width might not be reliable.

[b] Composite equivalent width.

[c] The large standard deviation is primarily due to one measure.

[d] Corrected for the presence of two continua.

TABLE 6B

Hα Equivalent Widths for the Stars with $\sigma_W \geq 0.060$ Å

Star Name	Date of Observation	W_α (Å)	R_c	W_{em} (Å)	Reference Star	Observatory Code
HD 12545	03/01/1985	+0.751	1.22	+1.857	μ Her	KPNO0.4
	03/04/1985	+0.992	1.23	+2.098		KPNO0.4
	03/05/1985	+1.961	1.40	+3.067		KPNO0.4
	03/15/1985	+0.895	1.27	+2.001		KPNO0.5
	09/30/1985	+0.963	1.21	+2.069		KPNO0.2
	10/03/1985	+0.189	1.13	+1.295		KPNO0.2
	10/04/1985	+0.182	1.13	+1.288		KPNO0.2
	11/08/1986	+1.352	1.45	+2.458		KPNO0.2
V711 Tau[a]	09/30/1985	+0.805	1.26	+1.919	δ Eri	KPNO0.2
	11/08/1986	+1.103	1.42	+2.217		KPNO0.2
	11/11/1986	+1.969	1.53	+3.083		KPNO0.2
EI Eri	08/23/1983	-0.311	0.877	+0.990	μ Her	2.1McD0.42
	08/24/1983	-0.817	0.770	+0.484		2.1McD0.42
	08/25/1983	-0.341	0.868	+0.960		2.1McD0.42
	08/26/1983	-0.486	0.832	+0.815		2.1McD0.42
BD+26°730	03/01/1985	+0.183	1.16	+0.748	61 Cyg B	KPNO0.4
	10/22/1988	+0.391	1.291	+0.956		KPNO0.18
	10/23/1988	+0.453	1.345	+1.018		KPNO0.18
12 Cam	03/06/1988	-1.250	0.477	-0.113	β Gem	Ritter0.3
	03/12/1988	-1.049	0.475	+0.088		Ritter0.3
IL Hya	01/22/1981	-0.232	0.819	+0.837	β Gem	2.7McD0.35
	05/01/1983	-0.431	0.727	+0.638		2.1McD0.42
	02/24/1986	-0.325	0.764	+0.744		2.1McD0.28
	02/27/1986	-0.402	0.744	+0.667		2.1McD0.28
	05/01/1986	-0.540	0.659	+0.529		2.1McD0.28
LQ Hya	04/30/1983	-0.172	0.881	+0.838	HR 166	2.7McD0.35
	05/01/1983	-0.099	0.946	+0.911		2.1McD0.42
	05/02/1983	-0.190	0.878	+0.820		2.1McD0.42
	05/01/1986	+0.011	1.022	+1.021		2.1McD0.28
	02/24/1986	-0.097	0.946	+0.913		2.1McD0.28
	02/26/1986	-0.047	0.933	+0.963		2.1McD0.28
	02/27/1986	+0.035	1.046	+1.045		2.1McD0.28
Gliese 410	03/05/1985	≈0.	≈1.	+0.565	61 Cyg B	KPNO0.4
	03/13/1985	-0.159	0.768	+0.406		KPNO0.5
HD 106225	05/13/1981	+0.433	1.137	+1.520	β Gem	2.7McD0.35
	04/29/1983	+0.075	1.058	+1.162		2.1McD0.42
	04/30/1983	+0.064	≈1.	+1.151		2.1McD0.42
	02/24/1986	-0.601	0.652	+0.486		2.1McD0.28
σ^2 CrB[a]	05/27/1988	-1.392	0.640	+0.178	β Com	Ritter0.3
	06/04/1988	-1.427	0.634	+0.143		Ritter0.3
	06/06/1988	-1.298	0.662	+0.272		Ritter0.3
	06/10/1988	-1.327	0.643	+0.243		Ritter0.3
	06/11/1988	-1.395	0.630	+0.175		Ritter0.3
	06/13/1988	-1.426	0.617	+0.144		Ritter0.3
	06/20/1988	-1.219	0.624	+0.351		Ritter0.3
	06/27/1988	-1.046	0.668	+0.524		Ritter0.3
	06/27/1988	-1.018	0.656	+0.552		Ritter0.3
	06/27/1988	-1.154	0.683	+0.416		Ritter0.3
	06/28/1988	-1.249	0.640	+0.321		Ritter0.3
	06/30/1988	-1.302	0.729	+0.268		Ritter0.3
	06/30/1988	-1.297	0.709	+0.273		Ritter0.3
	07/01/1988	-1.152	0.715	+0.418		Ritter0.3
	07/02/1988	-1.476	0.699	+0.094		Ritter0.3
	07/05/1988	-0.970	0.663	+0.600		Ritter0.3
HR 6469[a]	04/30/1987	-1.384	0.377	-0.124	μ Her	Ritter0.3
	05/05/1987	-1.094	0.485	+0.166		Ritter0.3
	05/09/1987	-1.226	0.403	+0.034		Ritter0.3
	06/17/1987	-1.285	0.400	-0.025		Ritter0.3
29 Dra	04/29/1983	-0.748	0.561	+0.292	β Gem	2.1McD0.42
	05/02/1983	-0.767	0.552	+0.273		2.1McD0.42
	08/23/1983	-0.562	0.635	+0.478		2.1McD0.42
	08/25/1983	-0.048	0.906	+0.992		2.1McD0.42
	08/27/1983	-0.342	0.728	+0.698		2.1McD0.42
	07/05/1988	-0.772	0.602	+0.365		Ritter0.3
	07/13/1988	-0.694	0.607	+0.443		Ritter0.3
	10/23/1988	-0.641	0.534	+0.399		KPNO0.18

TABLE 6B—*Continued*

Star Name	Date of Observation	W_α (Å)	R_c	W_{em} (Å)	Reference Star	Observatory Code
HR 7275	05/17/1987	-0.504	0.666	+0.683	α Boo	Ritter0.3
	07/29/1987	-0.549	0.617	+0.638		Ritter0.3
	08/12/1987	-0.817	0.561	+0.370		Ritter0.3
	08/18/1987	-0.723	0.544	+0.464		Ritter0.3
	09/06/1987	-0.741	0.557	+0.446		Ritter0.3
	09/15/1987	-0.865	0.486	+0.322		Ritter0.3
	09/27/1987	-0.939	0.497	+0.248		Ritter0.3
	10/19/1987	-0.868	0.514	+0.319		Ritter0.3
	10/28/1987	-0.779	0.535	+0.408		Ritter0.3
	11/06/1987	-0.917	0.486	+0.270		Ritter0.3
	12/31/1987	-0.823	0.548	+0.364		Ritter0.3
	07/01/1988	-0.897	0.565	+0.290		Ritter0.3
	07/02/1988	-0.692	0.603	+0.495		Ritter0.3
	07/03/1988	-0.842	0.547	+0.345		Ritter0.3
	07/05/1988	-0.750	0.550	+0.437		Ritter0.3
	07/13/1988	-0.746	0.584	+0.441		Ritter0.3
	07/14/1988	-0.931	0.520	+0.256		Ritter0.3
	08/21/1988	-0.739	0.593	+0.448		Ritter0.3
	08/26/1988	-0.738	0.555	+0.449		Ritter0.3
	09/08/1988	-0.728	0.570	+0.459		Ritter0.3
HR 8703	10/04/1987	-0.438	0.712	+0.577	β Oph	Ritter0.3
	10/04/1987	-0.520	0.671	+0.495		Ritter0.3
	10/14/1987	-0.700	0.591	+0.315		Ritter0.3
	10/19/1987	-0.668	0.633	+0.347		Ritter0.3
	10/28/1987	-0.184	0.854	+0.831		Ritter0.3
	11/04/1987	-0.702	0.590	+0.313		Ritter0.3
	11/06/1987	-0.575	0.680	+0.332		Ritter0.3
	11/13/1987	-0.884	0.540	+0.131		Ritter0.3
	12/30/1987	-1.015	0.493	0.000		Ritter0.3
II Peg	11/08/1986	+0.350	1.22	+1.399	δ Eri	KPNO0.2
	11/11/1986	+0.605	1.41	+1.654		KPNO0.2

[a] Equivalent width of the composite line is given.

early F star (most likely a subgiant) and a G5 giant (Fig. 4). Any H and K emission from the late-type star would be substantially diluted by the F star continuum.

BD +26°730 = V833 Tau.—Hα is a variable emission feature (Table 6B and Fig. 4). Hε seems also to be in emission but is blended with the Ca II H emission line.

HD 30957.—A recently discovered double-lined spectroscopic binary (F. C. F.; see entry in the CABS catalog). Our Ca II observation shows strong H and K emission at a flux level of log $\mathscr{F}$(K) ~ 6.6 and a weak Hα absorption line filled in by chromospheric emission.

HD 31738.—This is also a newly discovered double-lined spectroscopic binary with very strong Ca II emission lines of log $\mathscr{F}$(K) ~ 6.8, presumably from the G5 IV primary. Hε might be an emission feature. Our observations of the Hα region show Hα to be a very weak, almost absent, absorption feature filled in by chromospheric emission.

HD 31993.—Moderately strong Ca II H and K emission lines indicate activity, while Hα appears as a strong absorption line. Its equivalent width is about 300 mÅ larger than the value for the reference star β Oph.

12 Cam.—The Hα absorption line may show variable filling (Table 6B), but this needs to be confirmed.

HD 33798.—This star is a rapidly rotating single K0 giant with strong Ca II emission lines at a flux level of log $\mathscr{F}$(K) ~ 6.3. Hα appears to be a normal absorption feature comparable to that of the reference star β Gem. A high-resolution 6430 Å CCD spectrum shows rotationally broadened lines of 29 ± 2 km s^{-1}.

HD 34198.—Another rapidly rotating single K0 giant with moderately strong H and K emission but very strong Hα absorption.

HR 1908.—Being among the latest-type giants in this sample (K4), HR 1908 shows weak H and K emission lines at a normal flux level of log $\mathscr{F}$(K) ~ 5.0. Hα seems to be also a normal absorption feature or, at most, very weakly filled in by emission if compared, e.g., with the K4 III reference star β Cnc (Table 6A).

χ^1 Ori.—Although the H and K emission lines of this G0 dwarf star are only marginally visible in our 0.5 Å resolution spectrum in Figure 10, the star has a fairly large emission-line flux level of log $\mathscr{F}$(K) ~ 6.6. From our six Hα region spectra Hα appears to be a normal and constant absorption feature.

HR 2081.—This star is a double-lined spectroscopic binary with a relatively long orbital period of 219 days (Beavers and Griffin 1979). Our H and K flux measure in Table 3 is approximately the lower limit for reliable fluxes from the DAO 0.9 Å spectra. Higher resolution spectra are needed to determine a more accurate flux. Hα is a very strong absorption feature even if compared with the reference star o UMa.

1 Gem.—Basri, Laurent, and Walter (1985) list the period of this system as 9.6 days with spectral type of F5 V + G5 II and note that the spectral type of the secondary (the F star) is estimated from an ultraviolet spectrum. Thus, they imply that the system is a double-lined binary with a 9.6 day period. In fact the system is triple. The mid-F star which dominates the ultraviolet is the primary of the 9.6 day binary whose secondary is undetected. Thus, it is unlikely to be particularly chromospherically active. The continuum of the late-type star, a K0 III, dominates at yellow and red wavelengths. This component has an orbital period of 13.4 yr. See Griffin and Radford (1976) for further discussion. Thus, substantial chromospheric activity from this component is also unexpected. The flux of the K line bottom does not exceed log $\mathscr{F}$(K) ~ 5.3. Hα seems to be a normal absorption line.

OU Gem = HD 45088.—This star is known double-lined spectroscopic binary with an orbital period of 7 days (Tomkin 1980). Ca II H and K emission is evident from the 0.9 Å spectrum in Figure 10 but higher resolution spectra are needed to resolve the emission from both components for a more accurate flux determination. One 0.2 Å Hα region spectrum shows double Hα absorption lines (Fig. 4) with a line ratio of K5/K3 = 0.43 ± 0.02 for photospheric lines and 0.32 for Hα.

σ Gem.—Probably variable Ca II H and K emission.

HD 65195.—Our Ca II H and K spectra show weak emission lines but a flux level of log $\mathscr{F}$(K) ~ 6.1. The star is one of the single-lined spectroscopic binaries listed in the "candidate table" in the CABS catalog which turned out to be chromospherically active. Hα appears to be a normal absorption feature or, at most, weakly filled in by chromospheric emission.

54 Cam.—The H and K emission lines are blueshifted in our spectrum in Figure 10 but unshifted (or even slightly redshifted) on other spectra. Although this is a double-lined spectroscopic binary whose components have similar line strengths, only one component appears to have Ca II H and K emission. This system is of particular interest because the estimated spectral type of F9 IV for both components is quite early for a chromospherically active star. We note, however, that Wolff, Boesgaard, and Simon (1986) found that onset of "activity" in stars on or near the main sequence occurs approximately at spectral type F0. The listed Hα equivalent width is measured from the composite spectrum and is fairly weak if compared to the reference star η Boo.

28 Mon.—Our six Hα spectra show a normal absorption profile with slightly larger equivalent width if compared to the reference star β Cnc. Ca II H and K emission seems to be present but our spectrum has insufficient signal-to-noise ratio (Fig. 10) to compute a reliable flux.

35 Cnc.—Two 0.5 Å and 0.9 Å resolution Ca II observations did not reveal any emission lines. Bopp, Dempsey, and Maniak (1988) report a very strong Hα absorption line.

π^1 UMa.—A single G0 dwarf with weak Ca II H and K emission lines but fairly high line flux of log $\mathscr{F}$(K) ~ 6.5. No Hα observation has been obtained.

HD 80715.—Both components show strong Ca II H and K emission lines. Balmer Hε emission from both component is also evident. Barden and Nations (1988) report Hα emission from both components (Table 6A), with one of them variable.

IL Hya = HD 81410.—Strong Ca II H and K emission, weak and variable Hα absorption, possible Hε emission, and photometric variability make this system a good candidate for a monitoring program.

24 UMa.—Our Ca II observation show only weak H and K emission lines but a moderately strong flux level of log $\mathscr{F}$(K) ~ 6.2. Recent Hα observations by Bopp, Dempsey, and Maniak (1988) reveal a normal absorption feature when compared to the reference star μ Her.

LQ Hya = HD 82558.—Very strong Ca II H and K emission and also strong Hϵ emission at a flux level of log $\mathscr{F}$(Hϵ) ~ 6.7.

HD 86856.—Strong Ca II H and K emission. Hϵ also might be in emission. Hα is a very strong absorption feature, approximately 100 mÅ stronger than the K7 V reference star 61 Cyg B.

LR Hya = HD 91816.—The H and K emission line in our Ca II spectrum in Figure 10 is a composite from the two K0 dwarf components. The Hα region spectra, taken at a different phase than the Ca II observation, show two very weak filled-in Hα absorption lines.

Gliese 410.—Another dMe star with strong Ca II H and K emission. One of our Hα spectra show the Hα line in absorption while in another spectrum Hα is completely filled in (Table 6B).

ξ UMa B.—Ca II H and K emission is rather weak but the flux level reaches log $\mathscr{F}$(K) ~ 6.3. Our one Hα region spectrum shows an absorption feature slightly filled in by chromospheric emission.

HR 4430.—This 75 day single-lined spectroscopic binary is apparently only a very weakly "active" system, if at all. The 0.24 Å CCD observation in Figure 10 shows weak H and K emission at a flux level of only log $\mathscr{F}$(K) ~ 5.7. From 10 Hα region spectra, Hα appears to be a very strong absorption feature with an equivalent width of approximately 280 mÅ *larger* than the K2 III reference star β Oph.

DF UMa.—The visual component (ADS 8242B) is also a dM star with weak Ca II emission and forms together with DF UMa a spectroscopic triple system containing three dM stars. Although listed in Table 6A, there is a lot of Hα variability of the composite emission line. Thus, we did not use this star in the analysis. Figure 10 shows strong Hϵ emission.

61 UMa.—A fairly active single G8 dwarf star with log $\mathscr{F}$(K) ~ 6.3 but strong Hα absorption (160 mÅ in excess compared to the reference star HR 166).

HD 106225.—Very active RS CVn system with log $\mathscr{F}$(K) ~ 6.7 and also variable Hα absorption line profile (Table 6B).

31 Com.—Very hard to measure at Ca II H_1 and K_1 due to almost absent emission lines. The emission flux level is nevertheless very high [log $\mathscr{F}$(K) ~ 6.6]. Bopp, Dempsey, and Maniak (1988) report very strong Hα absorption. Note, our $v \sin i$ value of 57 km s^{-1} is substantially less than the value of 80 km s^{-1} given in Uesugi and Fukuda (1982) from six references. This may be because the broad lines are less blended with other features in our red wavelength spectra, while the other determinations were made in the blue.

HD 113983.—Very likely not an active system.

HD 115781.—This star is listed in the "candidate table" in the CABS catalog because no observations of activity indicators were made. Our three Ca II H and K spectra show strong emission lines at a flux level of log $\mathscr{F}$(K) ~ 6.4. Hα appears to be a normal absorption feature.

HD 116204.—Very active RS CVn system with log $\mathscr{F}$(K) ~ 6.5 and filled-in Hα absorption.

HD 116378.—Although the H and K emission-line strengths are very weak (compare our spectrum in Fig. 10), the emission-line fluxes are typical of chromospherically active stars [log $\mathscr{F}$(K) ~ 6.4]. Hα appears as a normal absorption feature.

FK Com.—Ca II K line surface flux of log $\mathscr{F}$(K) ~ 7.3! Walter and Basri (1982) and others reported a very broad and variable Hα emission line with equivalent widths of sometimes up to 10 Å!

HR 5110.—The Hα profile is clearly composite, from an F star and a K star. The Ca II H and K emission from the K star is decreased by the addition of the F star's continuum (Fig. 10).

4 UMi.—Although listed in the CABS catalog, our high-resolution Ca II CCD observation (Fig. 10) shows only very weak H and K emission at a flux level of log $\mathscr{F}$(K) ~ 5.3, thus the star should *not* be considered as chromospherically active.

HR 5534.—This is a new CA star having H and K emission at a flux level of log $\mathscr{F}$(K) ~ 6.4. Six Hα region spectra show a constant but filled-in Hα absorption line.

HR 5553.—Four Ca II spectra show moderate H and K emission lines of log $\mathscr{F}$(K) ~ 6.15, while 14 Hα region observations reveal a strong Hα absorption feature which might be variable.

δ CrB.—Bopp, Dempsey, and Maniak (1988) report normal Hα absorption (see also Table 6A). From three Ca II spectra we find moderate emission-line fluxes of log $\mathscr{F}$(K) ~ 6.1.

HD 143313.—The star is listed as a chromospherically active double-lined binary star in the CABS catalog without having a Ca II H and K observation. Our one observation shows strong (composite) emission lines at a flux level of log $\mathscr{F}$(K) ~ 6.6 and thus verifies its chromospheric activity.

σ^2 CrB.—Together with FK Com and LQ Hya, σ^2 CrB is another system having Ca II K emission-line flux greater than 10^7 ergs cm^{-2} s^{-1}. The system is, however, a double-lined spectroscopic binary with two rapidly rotating components. From 16 Hα observations we find the line to be variable and filled-in.

29 Dra.—Ca II H and K emission above the continuum; log $\mathscr{F}$(K) ~ 6.4 from one 0.9 Å spectrum. Hα is a weak and variable absorption feature (Table 6B).

V775 Her = HD 175742.—Strong Ca II H and K emission. Balmer Hϵ emission of log $\mathscr{F}$(Hϵ) ~ 6.5. Hα is a weak, filled-in absorption line.

HR 7275.—Bopp (1984) reported strong Ca II H and K emission of log $\mathscr{F}$(K) ~ 6.5 (Table 7). Our Hα monitoring reveals a weak and variable absorption line profile (Table 6B).

HD 185151.—Broad H and K emission lines of log $\mathscr{F}$(K) ~ 6.3. Hα appears to be a normal absorption line if compared to the reference star α Boo.

HD 191262.—Our 0.3-Å CCD spectrum in Figure 10 shows double Ca II H and K emission lines of log $\mathscr{F}$(K) ~ 6.5 for each component.

HR 8703.—Strong Ca II H and K emission lines well above the continuum at a flux level of log $\mathscr{F}$(K) ~ 6.4. Hα monitoring reveals a quite variable and weak absorption line profile (Table 6B).

λ And.—Three Ca II H and K observations show no significant flux variability.

HR 9024.—Weak H and K emission lines but flux level of log $\mathscr{F}$(K) ~ 6.7. Three Hα region spectra show a normal absorption line feature comparable to that of the reference star o UMa.

Table 8 of the CABS catalog listed 37 candidate stars. For most of these systems, either their binary nature was unknown or questioned or there was no observation of Ca H and K emission. From our present Ca H and K observations we confirm that 5 of the candidate stars, HD 19485, HD 30957, HD 65195, HD 115781, and HD 191262, are chromospherically active binaries, according to the CABS catalog definition. If HR 1176 = HD 23838 has a composite spectrum with an early-type secondary, the emission is probably strong enough to include this star in the catalog. Thus, it remains on the candidate list. The emission of HR 1023 = HD 21018 is probably too weak to include this star in the catalog. Finally, one star, HR 1455 = HD 29104, shows no Ca H and K emission and should be rejected from the catalog.

V. DISCUSSION AND ANALYSIS

a) Effect of Limited Sampling

The stars in this sample have been observed on average about 2 times at H and K and about 2–3 times at Hα, but there are many stars which have only one observation: from the total of 83 stars observed at H and K, 54 were observed only once and from the 96 stars observed at Hα, 37 had only a single observation. For example, out of the 34 chromospherically active stars which were observed more than twice at Hα, 14 stars showed large equivalent width variations with a standard deviation in excess of 60 mÅ. That is approximately 40% of those stars. We can say even less about Ca II H and K variability because only few stars have been observed more than twice. How does this affect the analysis? The Ca II H and K solar neighborhood survey (e.g., Vaughan and Preston 1980; Soderblom 1985) showed rotational modulation of the H and K emission of up to 10% and long-term activity cycles with amplitudes up to 30%, in addition to the observational error. Moreover, since the stars in the present sample are mostly very active systems, larger rotational modulations than those found for the solar-type dwarfs of the solar neighborhood survey are likely.

Thus, deriving quantitative relationships between activity indicators and other stellar parameters for very active stars is quite dangerous and needs longer time baseline and substantially increased sampling. Nevertheless, we may search for qualitative relations and trends in the data.

b) Dependence of Activity on Temperature

It has been argued (e.g., Basri 1987; Rutten and Schrijver 1987) that R_{HK} is not the appropriate parameter to describe chromospheric activity, mostly because no tight correlations were found when it was plotted versus the rotation period. Figure 5*a* is a plot of the mean values of the sum of the unnormalized Ca II H and K line fluxes corrected for photospheric contribution, $\mathscr{F}'$(H+K), versus effective (photospheric) temperature. Also included in Figure 5*a* is the slope of the best fit to the data (*dashed lines*), labeled on the left side with T^3. Note that effective temperature has been always taken from the spectral type–effective temperature tables in Landolt-Börnstein (Schmidt-Kaler 1982; and references therein). $\mathscr{F}'$(H+K) declines toward cooler effective temperature. This trend emerges despite wide scatter in $\mathscr{F}'$(H+K) at each spectral type and, presumably, wide scatter in rotation velocity or period at each type. Therefore, caution is required when comparing $\mathscr{F}'$(H+K) between stars of similar rotation velocity or period but different spectral type. The dotted line is the slope of the best fit found by Kelch, Linsky, and Worden (1979) for the Ca II K line fluxes of 14 stars, $K_1(\text{corr.}) \approx T_{\text{eff}}^{3.7}$.

Figure 5*b* is a plot of the Ca II H and K radiative losses in units of the bolometric flux, R_{HK}, i.e., the fraction of the stellar luminosity which appears as emission in the H and K lines,

$$R_{HK} = \frac{\mathscr{F}'(H_1) + \mathscr{F}'(K_1)}{\sigma T_{\text{eff}}^4}, \tag{7}$$

versus effective temperature. The $\sim T^3$ decline toward cooler stars is now gone, the scatter is real, and the gap can be seen running horizontally at $R_{HK} \sim 2\text{–}4\times10^{-5}$, which we have used to divide the stars up into "quiet" and "active" chromosphere stars for the entry in Table 2. We may identify this gap as the well-known Vaughan-Preston gap (Vaughan and Preston 1980). It has been suggested by several authors (e.g. Middelkoop 1982) that this gap indicates a discontinuous change in the chromospheric characteristics at a certain age or rotation rate. Assuming a smoothly varying decay of chromospheric activity with age, Hartmann *et al.* (1984) showed that there is no need for a discontinuous change in the chromospheric behavior to explain the Vaughan-Preston gap. Our data of mostly "overactive" single and binary stars—dwarfs, subgiants, and giants—show the gap for stars with $T_{\text{eff}} > 4300$ K (α K3 III or K5 V) somewhat clearer than for cooler stars. Rutten (1987) explains an "absence" of the gap for cooler stars with a color-dependent shape of the activity-rotation relation.

Figure 5*c* shows the situation for Hα. Plotted is the core emission equivalent width described in § III*c*. The vertical bars indicate the variations of stars listed in Table 6B. No clearly visible temperature dependence seems to be present.

We have also used Simon and Fekel's (1987) C IV line fluxes (their Table 1) of 67 single stars and single-lined spectroscopic binaries in common with our program stars to evaluate their slope. A variety of slopes ranging from T^3 to T^{10} are plotted in Figure 5*d* for comparison purposes. No quantitative fit is possible, but it seems clear that there is a general increase in C IV emission-line flux with temperature by $\mathscr{F}(\text{C IV}) \approx T_{\text{eff}}^{7\cdots10}$. As a comparison, Linsky and Ayres (1978) found for the Mg II *k* line fluxes of 29 stars a temperature dependence of $\mathscr{F}'(k_1) \approx T_{\text{eff}}^7$.

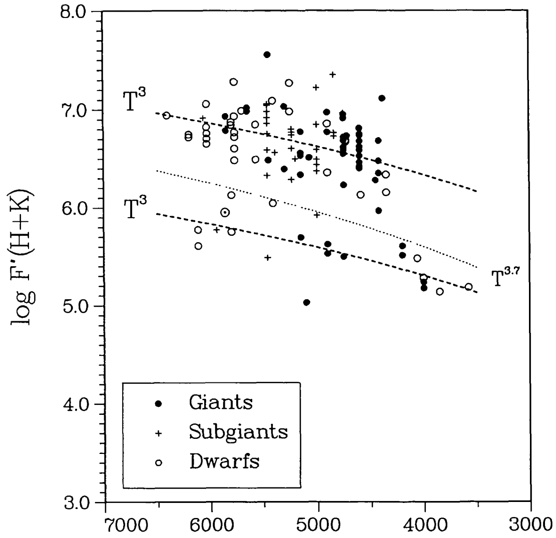

FIG. 5*a*

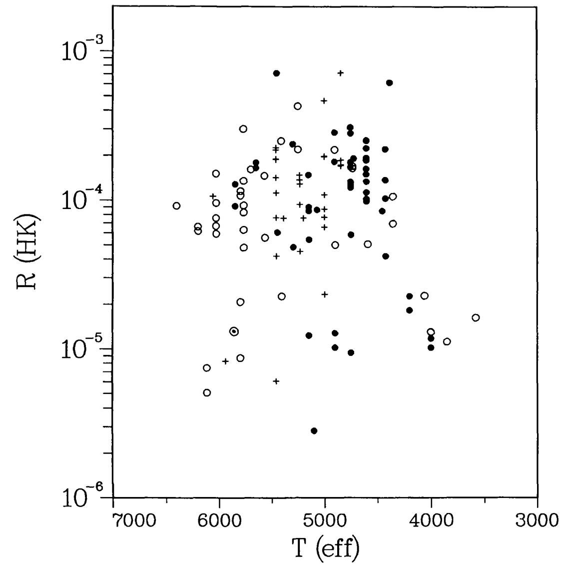

FIG. 5*b*

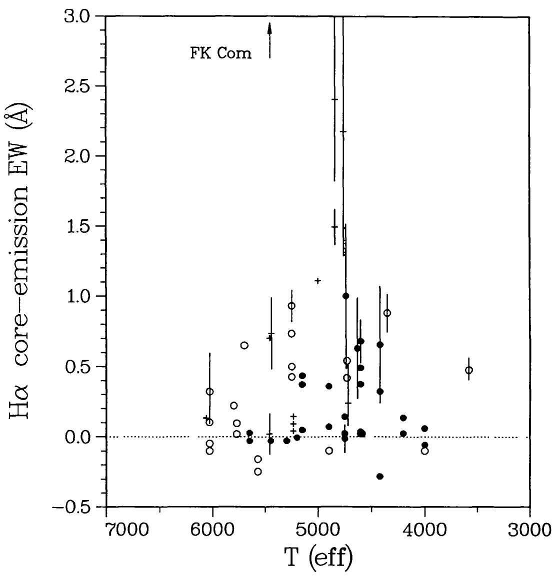

FIG. 5*c*

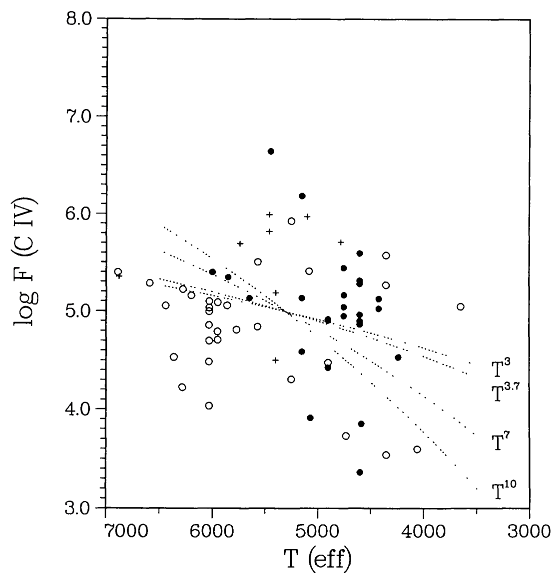

FIG. 5*d*

FIG. 5.—Temperature-activity relations for the full sample. (*a*) Plotted is the sum of the corrected H_1 and K_1 indices, log $\mathcal{F}'$(H+K), vs. T_{eff}. Indicated is the T^3 slope (*dashed lines*) for the active and nonactive stars as discussed in the text. Also shown is Kelch *et al.*'s (1979) $T^{3.7}$ slope (*dotted line*) for comparison purposes. This line has been arbitrarily shifted for better display. The Sun is also indicated (⊙). (*b*) R_{HK} vs. T_{eff}. (*c*) Hα core emission equivalent width vs. T_{eff}. The vertical bars indicate the range of Hα variations seen in some of the stars (Table 6B). The mean Hα emission equivalent width for FK Com is 3.3 Å (Walter and Basri 1982) but is highly variable (values up to 10 Å were measured). This is schematically indicated by the arrow. (*d*) log $\mathcal{F}$(C IV) vs T_{eff}. The stars plotted are the same ones as in the other panels. C IV emission-line fluxes have been taken from Simon and Fekel (1987). Several temperature slopes are indicated. Note that the active stars lie well above the $T^{7\cdots10}$ trend of most of the inactive and less active stars.

c) *Dependence of Activity on Rotation*

Rutten and Schrijver (1987) reject the use of the convective turnover time, τ_c, to scale the rotation period as introduced by Noyes *et al.* (1984), mostly because it introduces model-dependence but also because $\mathcal{F}$ versus P for several UV ions shows the same amount of scatter as the relation $\mathcal{F}$ versus P/τ_c. In this paper we follow this precept and use directly the rotation periods as derived from broad-band photometric variations or H and K$\langle S \rangle$ index variations. Note that some stars have been plotted with a rotation period derived from $v \sin i$. These approximate periods are computed from our $v \sin i$ measures as indicated in Table 2 with stellar radii from the Landolt-Börnstein tables (Schmidt-Kaler 1982), and cor-

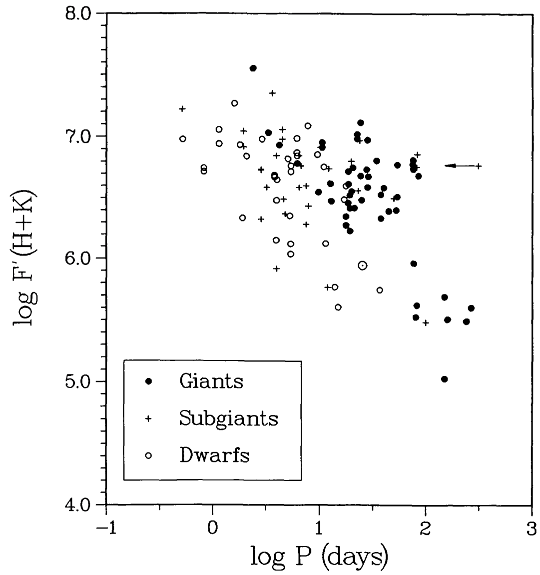

FIG. 6*a*

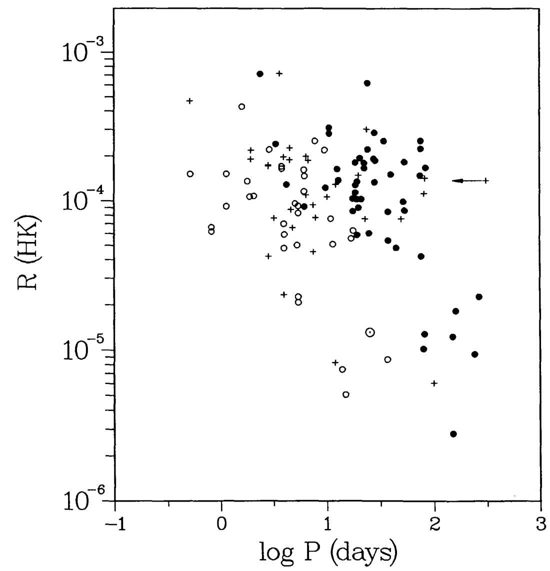

FIG. 6*b*

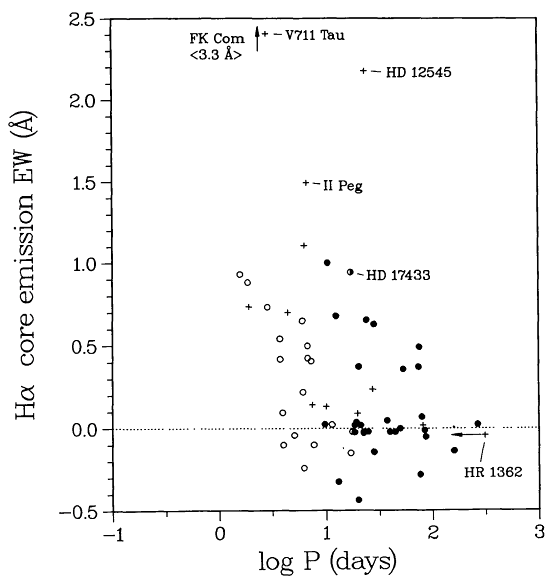

FIG. 6*c*

FIG. 6.—Rotation-activity relations. (*a*) log $\mathcal{F}'$(H + K) vs. rotation period *P*. The subgiant to the right is HR 1362; its arrow head indicates half of the measured period (see text). The Sun is indicated as ⊙. (*b*) R_{HK} vs. rotation period. (*c*) Hα core emission equivalent width vs. rotation period. The arrow indicates the position of FK Com with an Hα equivalent width mean value of 3.3 Å. The subgiant in the upper right part, HD 12545, is plotted with the orbital period of 23.9 days.

recting for $\langle \sin i \rangle = \pi/4$

$$P_{\rm rot}(v \sin i) = 39.7 \frac{R}{v \sin i}, \qquad (8)$$

where the period *P* is in days, the radius *R* in solar radii, and $v \sin i$ in km s^{-1}. In the case of short-period binaries without a photometric period determination, we have assumed synchronization and used their orbital periods (Table 2). The unnormalized Ca II H and K fluxes are plotted against rotation period *P* in Figure 6*a*. Excluded are double-lined spectroscopic binaries with composite emission lines; included are some stars taken from the literature and listed in Table 7 in the Appendix. No single relation can be employed for all luminosity classes. There is clear evidence that evolved stars are generally more active than main-sequence stars of the same rotation period. Perhaps this really means that surface rotational velocity is the more relevant parameter, since the giants must be rotating faster than dwarfs if the rotation periods are equal.

Another interesting feature in Figure 6*a* is the discontinuity in the surface flux at log $\mathcal{F}$(H + K) ~ 6.0 for the giant stars (but less pronounced for the dwarf stars). For comparison purposes we have plotted R_{HK} in Figure 6*b*. These data are also in agreement with the expected trend that more rapidly rotating stars have larger R_{HK} but there appears to be a stronger segregation of evolved and unevolved stars plus additional scatter partially introduced by the uncertainties of the spectral type–$T_{\rm eff}$ relation. The gap, however, is more visible in the R_{HK}–log *P* plane. We may speculate that this gap represents the onset of chromospheric activity in evolved stars at almost exactly 80 days. An interesting star in Figures 6*a* and 6*b* is HR 1362, a single G8 subgiant, with a (photometric) rotation period of ≈ 310 days (Strassmeier and Hall 1988) and very strong Ca II H and K emission. It is however not absolutely clear if the 310 day period or half of that is the correct period (this is indicated in Fig. 6 with an arrow). No matter which rotation period is the correct one, it is currently the longest known for a chromospherically active star and does not fit in the above mentioned trend.

The Hα activity-rotation relation (Fig. 6*c*) is quite similar to that of the Ca II surface fluxes. This is not surprising since both lines originate at approximately the same temperature

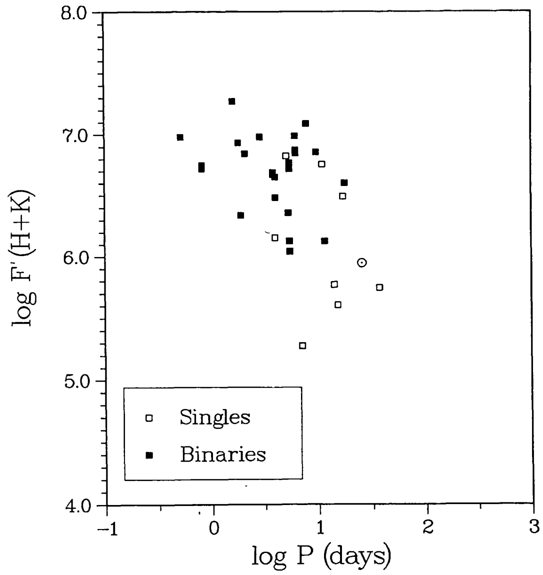

FIG. 7*a*

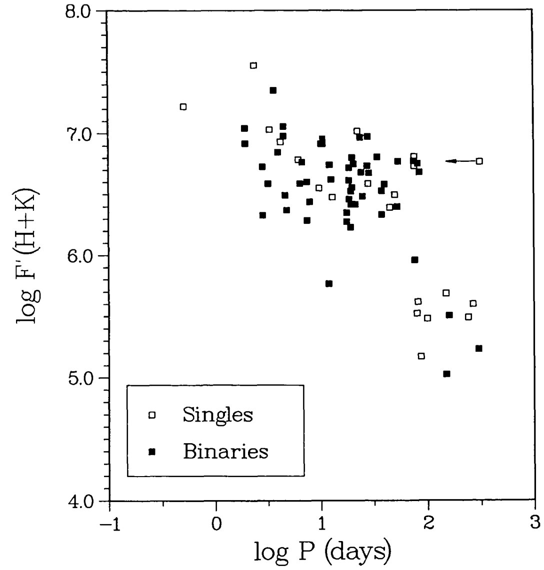

FIG. 7*b*

FIG. 7.—The role of duplicity in the rotation-activity relation (*a*) for main-sequence stars and (*b*) for evolved stars. The filled symbols indicate binaries; the open symbols, single stars. The Sun is indicated as ⊙, and the arrow indicate $1/2P_{\rm phot}$ for HR 1362. The most active unevolved stars are all members in binary systems, while the most active evolved stars can be found in binaries as well as single stars. The two very active, evolved single stars in the upper left-hand corner are HD 36705 (at log $P \sim -0.25$) and FK Com. The two binary stars in the right panel within the activity gap at log $\mathscr{F}$(H+K) ~ 6.0 are η Boo (log $P \sim 1.0$) and HR 4430 (log $P \sim 2.0$). Both stars are problematic entries for this figure since the rotation period of η Boo is derived from $v \sin i$ and an assumption for the radius, while HR 4430 is plotted with the orbital period of 75 days.

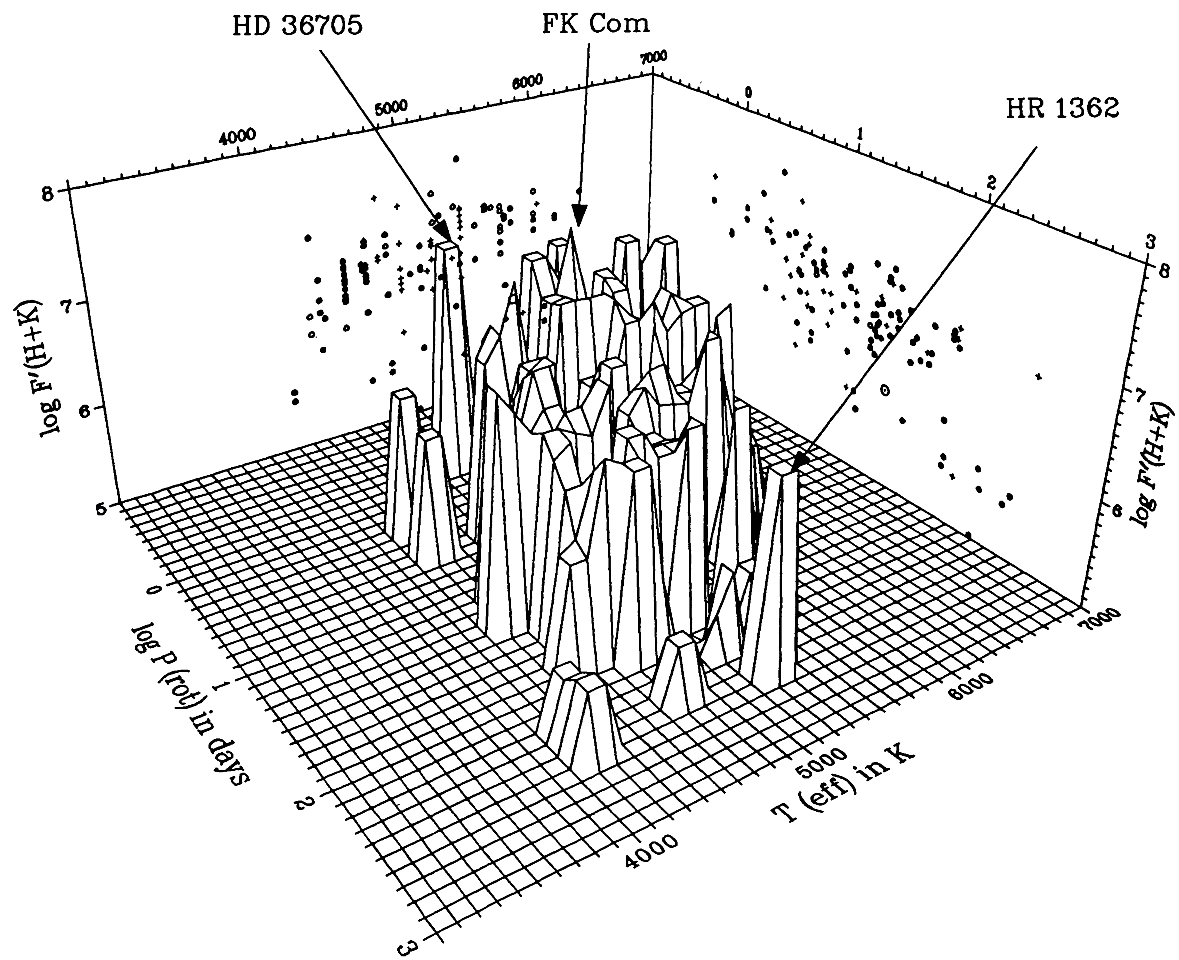

FIG. 8.—Full sample in the temperature-rotation-activity space. Three outstanding systems have been marked. Note the general decline of activity with rotation *and* temperature.

level in the chromosphere. Figure 6*c* also shows the same trend as the Ca II data in that the evolved stars are more active than their main-sequence counterparts for the same rotation period. The arrow at the upper edge of the plot indicates the position of FK Com with a mean Hα emission of +3.3 Å (Walter and Basri 1982). HD 17433 was originally classified as a G9 dwarf but Bopp *et al.* (1989) revised its spectral type to a K3–4 star which is slightly above the main sequence. Another interesting star in Figure 6*c* is the single-lined G5 IV binary star HD 12545 which has quite strong Hα emission. However, note that, since no rotation period has been observed, we have assumed synchronization and used the orbital period (24 days) as the rotation period which might turn out to be not true. Also note that HR 1362 (arrow in the lower right-hand corner) is well within the expected activity-rotation trend—as opposed to its Ca II behavior.

Activity-rotation plots from the C IV line can be found in Rutten and Schrijver (1987), Simon and Fekel (1987), Simon, Herbig, and Boesgaard (1985) and others.

d) *Single Stars versus Binaries*

Shown in Figure 7 is the activity-rotation relation for the same data set as in Figure 6*a* but subdivided into unevolved and evolved, single and binary stars. The full sample displayed in Figure 7*a* and 7*b* consists of 23 unevolved and 52 evolved stars in binary systems, and 14 unevolved and 26 evolved single stars, respectively.

From this figure it is obvious that a cool evolved star in a close binary is more active than a single main-sequence star of the same rotation period (compare also with Fig. 6*a*). Basri, Laurent, and Walter (1985) arrived at the same conclusion using hotter (UV) diagnostics as activity indicators. While a main-sequence star in a binary system is generally more active than a single star (Fig. 7*a*), simply because it can have a higher rotation period due to tidal coupling, this is not true for the evolved stars. The plot of the observed sum of the surface fluxes in our evolved star subsample (Fig. 7*b*) shows single stars well mixed with binaries of the same rotation period.

e) *The $P_{rot} - T_{eff}$ Plane*

Simon, Herbig, and Boesgaard (1985) have shown that it might be possible to predict a star's age from the measured emission-line flux. They investigated a sample of solar-type stars of $B-V=0.6$ ($\langle M/M_{\odot}\rangle = 1.1$) and found a tight function between log R(C IV) and P_{rot}/τ_c and substituted this relation into a functional age–R(C IV) law derived from a modification of Duncan's (1981) calibration of lithium abundances. From the Mount Wilson H and K data Duncan (1984) found a nearly linear relationship between rotation and color within $1.5 < P_{rot} < 12$ days and $0.4 < B-V < 0.85$ for the Hyades main-sequence stars. Simon, Herbig, and Boesgaard (1985) used this relationship to check their predictions.

Our sample consists of unevolved stars within a mass range from 0.67 $M_{\odot}$ (K5) to 1.3 $M_{\odot}$ (F6) and evolved stars from, say, 1.0 $M_{\odot}$ to 3 $M_{\odot}$. Because almost all of our stars lack an age determination, we cannot repeat Simon *et al.*'s analysis scheme, but we may plot our sample in the $P_{rot} - T_{eff}$ plane and investigate its dependence upon activity. This is demonstrated in the pseudo–three-dimensional plot in Figure 8. Plotted is the above mentioned sample (stars of luminosity class V, IV, III, singles and binaries) in the temperature-rotation-activity space. The slope of the surface in this three-dimensional plot demonstrates the decline of activity [expressed as log $\mathscr{F}'$(H+K)] with slower rotation *and* cooler temperature. Due to the mix of stars of different evolutionary status and large mass range, we do not attempt to quantify this behavior. Instead we want point out some details in this figure: (1) the major trend is from the back upper corner to the front lower corner, i.e., from high temperature and fast rotation to low temperature and slow rotation; (2) note that no stars cooler than ≈4000 K are plotted due to a lack of measured rotation periods for the late K and early M dwarf stars in our sample; (3) also note the lack of hotter stars (≈6000 K) at long periods (≈100 days) and cooler stars at short periods (≈1 day); (4) several of the very active stars stand out from the general trend and have been marked (HD 36705, FK Com, and HR 1362).

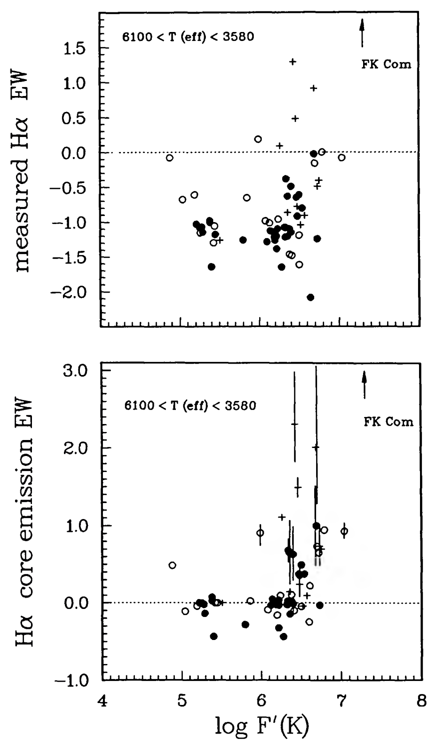

FIG. 9.—*Top panel:* Unnormalized CA II K flux in ergs cm^{-2} s^{-1} vs. measured Hα equivalent width (EW) in angströms, where the minus sign indicates absorption and the plus sign emission. *Lower panel:* Ca II K flux vs. Hα core emission EW. The arrow in both panels indicates the Hα EW of FK Comae with very strong and variable emission of +2 to +10 Å (Walter and Basri 1982). The group of stars at log $\mathscr{F}'$(K) ≈ 5.4 (*top panel*) are the Hα reference stars which were also measured at Ca II K. For stars with log $\mathscr{F}'$(K) > 6.0 there is a correlation between radiative loss in the K line and equivalent width of the Hα line. A puzzling point in the top panel is the rapidly rotating single G0 giant 31 Com with large radiative loss in the K line of log $\mathscr{F}'$ = 6.64 but strong Hα absorption of −2.1 Å.

f) *Observed* Ca II K – Hα *Diagram*

We now turn to Figure 9, the upper panel of which contains a plot of our measured core equivalent widths in angstroms (the minus sign is for absorption, the plus sign for emission) against unnormalized Ca II K line flux for giants (*dots*), subgiants (*pluses*), and dwarfs (*circles*). The lower panel of the figure is an identical plot for the determined Hα core emission equivalent width in Å (program star minus reference star). The vertical bars indicate the range of Hα variations of some of the stars from Table 6B (for clarity the bars are omitted in the upper panel and only the mean values are plotted).

Comparison of the distribution in the upper panel of Figure 9 with loci from model chromosphere calculations by Cram and Giampapa (1987), their Figure 2, suggests chromospheric temperatures of around 8000 K and a variety of different mass column densities. However, caution is in order if our data are compared to others because our "equivalent width" is defined so that it does not include the line wings. It is therefore somewhat smaller than the normally defined equivalent width. The trend in the measured Hα equivalent width–log $\mathscr{F}'$(Ca II K) plane (Fig. 9, *upper panel*) is that with increasing K line flux the Hα absorption core first *deepens* until log $\mathscr{F}'(K) \sim 5.8$ ergs cm^{-2} s^{-1} is reached and then *fills in* quite rapidly. This is exactly what one would expect from a simple one-component (isothermal) model chromosphere (Cram and Giampapa 1987).

We appreciate the careful reading of the manuscript by Mark S. Giampapa and his helpful comments. K. G. S. acknowledges the financial support of the Austrian Bundesministerium für Wissenschaft und Forschung and of the American Astronomical Society (Henri Chrétien Award). In addition, this project was partially supported by NASA grant NAG 8-111 to Tennessee State University. Research in stellar activity at the University of Toledo is supported by the National Science Foundation through grant AST 85-20542.

APPENDIX A

PREVIOUSLY PUBLISHED Ca II H AND K FLUXES INCLUDED IN THE ANALYSIS

We list in Table 7 previously measured values of the uncorrected emission-line fluxes, rotation periods, and effective temperatures for several stars in common with the present data set. A few additional stars are listed which have been included in our analysis. Note that some of these fluxes have been originally derived with another value for $V-R$ and differ therefore significantly from the fluxes listed in Table 3 (e.g., σ Gem) but have been recomputed using the same $V-R$ before plotting. The flux for Gliese 380 is a mean value from the two sources. We emphasize that Table 7 is not intended to give a complete listing of all previously published H and K fluxes.

TABLE 7

PREVIOUSLY PUBLISHED Ca II H AND K FLUXES FOR CHROMOSPHERICALLY ACTIVE STARS USED IN SOME OF THE ANALYSES IN THIS PAPER

Star Name	HD	log $\mathscr{F}(K_1)$ (ergs cm^{-2} s^{-1})	log $\mathscr{F}(H_1)$ (ergs cm^{-2} s^{-1})	P_{rot}[a] (days)	T_{eff}[b] (K)	Reference for $\mathscr{F}$
BD Cet	1833	6.49	6.52	34.46	4600	1
13 Cet	3196	...	6.57	2.082	5800	2
ζ And	4502	5.94	6.04	17.7692	4450	3
AY Cet	7672	6.43	6.32	77.22	5150	4
AR Psc	8357	6.46	6.46	12.245	5235	4
BD −0°210	8358	6.95	7.04	0.52	5770	5
VY Ari	17433	6.83	6.83	17.4[c]	5410	4
LX Per	...	6.11	5.93	7.905	5000	3
LX Per	...	6.38	6.35	7.905	5000	6
UX Ari	21242	6.63	6.53	6.438	5000	3
V711 Tau a	22468	6.46	6.41	2.841	4840	3
V711 Tau b	22468	6.05	6.12	2.841	5460	7
BD +26°730	...	6.04	5.97	1.9	4350	1
AB Dor	36705	6.92	...	0.514[d]	5000	2
TW Lep	37847	6.70	6.64	28.22	4900	4
BD +3°1007	37824	6.11	6.11	54.1[e]	4600	4
σ Gem	62044	5.85	5.76	19.410	4600	3
σ Gem	62044	5.77	5.73	19.410	4600	8
HR 3385	72688	5.98	5.91	19.34	4750	7
TY Pyx	77137	6.51	6.49	3.198	5460	3

TABLE 7—*Continued*

Star Name	HD	log $\mathscr{F}(K_1)$ (ergs cm^{-2} s^{-1})	log $\mathscr{F}(H_1)$ (ergs cm^{-2} s^{-1})	P_{rot}[a] (days)	T_{eff}[b] (K)	Reference for $\mathscr{F}$
IL Hya	81410	6.30	6.48	12.89	4600	3
24 UMa	82210	6.30	6.26	50.[f]	5200	3
Gliese 380	88230	4.99	4.96	...	4060	4, 9
DH Leo	86590	7.04	6.87	1.0665	4060	3
DK Dra a+b	106677	6.43	6.36	63.75	(4600)	3
AS Dra a	107760	5.72	5.91	5.415	5800	10
AS Dra b	107760	5.87	5.56	5.415	5410	10
BD +26°2347 a	108102	6.52	6.28	0.82	6200	10
BD +26°2347 b	108102	6.46	6.43	0.82	5200	10
UX Com	...	7.06	7.04	3.642	4840	10
RS CVn	114519	6.08	5.99	4.791	5000	3
RS CVn	114519	6.26	6.30	4.791	5000	10
σ^2 CrB a+b	146361	7.00	7.00	...	...	4
σ^2 CrB a	146361	6.61	6.67	1.168[e]	6400	10
σ^2 CrB b	146361	6.75	6.76	1.168	6030	10
WW Dra	150708	6.34	6.20	4.6296	5000	3
HR 6469	157482	6.62	6.53	81.9[e]	5460	4
Z Her	163930	5.63	5.61	3.97[e]	5000	10
V815 Her	166181	6.76	6.79	1.82[e]	5770	4
V815 Her	166181	6.64	6.62	1.82	5770	10
BY Dra a+b	234677	5.58	5.58	3.827	4060	4
HR 7275	179094	6.48	6.40	27.8	4720	4
V1764 Cyg	185151	5.52	5.38	40.3[e]	4600	4
BD +43°3759	199178	6.75	6.73	3.337[g]	5300	1
EQ Vir	...	5.92	5.80	3.96[h]	4350	8
RT Lac a+b	209318	6.62	6.59	5.074	5000	3
AR Lac a+b	210334	6.15	6.08	1.983	5000	3
V350 Lac	213389	6.04	6.08	17.755	4420	4
IM Peg	216489	6.86	6.78	24.39	4380	3
SZ Psc	219113	6.52	6.56	3.955	5000	3
SZ Psc	219113	6.58	6.57	3.955	5000	6
λ And	222107	6.23	6.23	53.95	5070	3
λ And	222107	6.23	6.20	53.95	5070	8
HR 9024	223460	6.66	6.72	22.61[i]	5650	4

[a] If not otherwise noted, taken from the CABS catalog.
[b] From the spectral type–T_{eff} relation in Landolt-Börnstein (Schmidt-Kaler 1982).
[c] Bopp *et al.* 1989.
[d] Lloyd-Evans 1987.
[e] Strassmeier *et al.* 1989.
[f] Period estimated from $v \sin i$.
[g] Bopp *et al.* 1983.
[h] Bopp and Fekel 1977.
[i] Strassmeier and Hall 1988.

REFERENCES.—(1) Bopp *et al.* 1983; (2) Pasquini *et al.* 1988; (3) Bopp 1983; (4) Bopp 1984; (5) Bopp *et al.* 1985; (6) Fernandes-Figuero *et al.* 1986*a*; (7) Smith 1984; (8) Linsky *et al.* 1979; (9) Giampapa *et al.* 1981; (10) Fernandes-Figuero *et al.* 1986*b*.

APPENDIX B

INDIVIDUAL Ca II H AND K SPECTRA FOR THE STARS LISTED IN TABLE 3

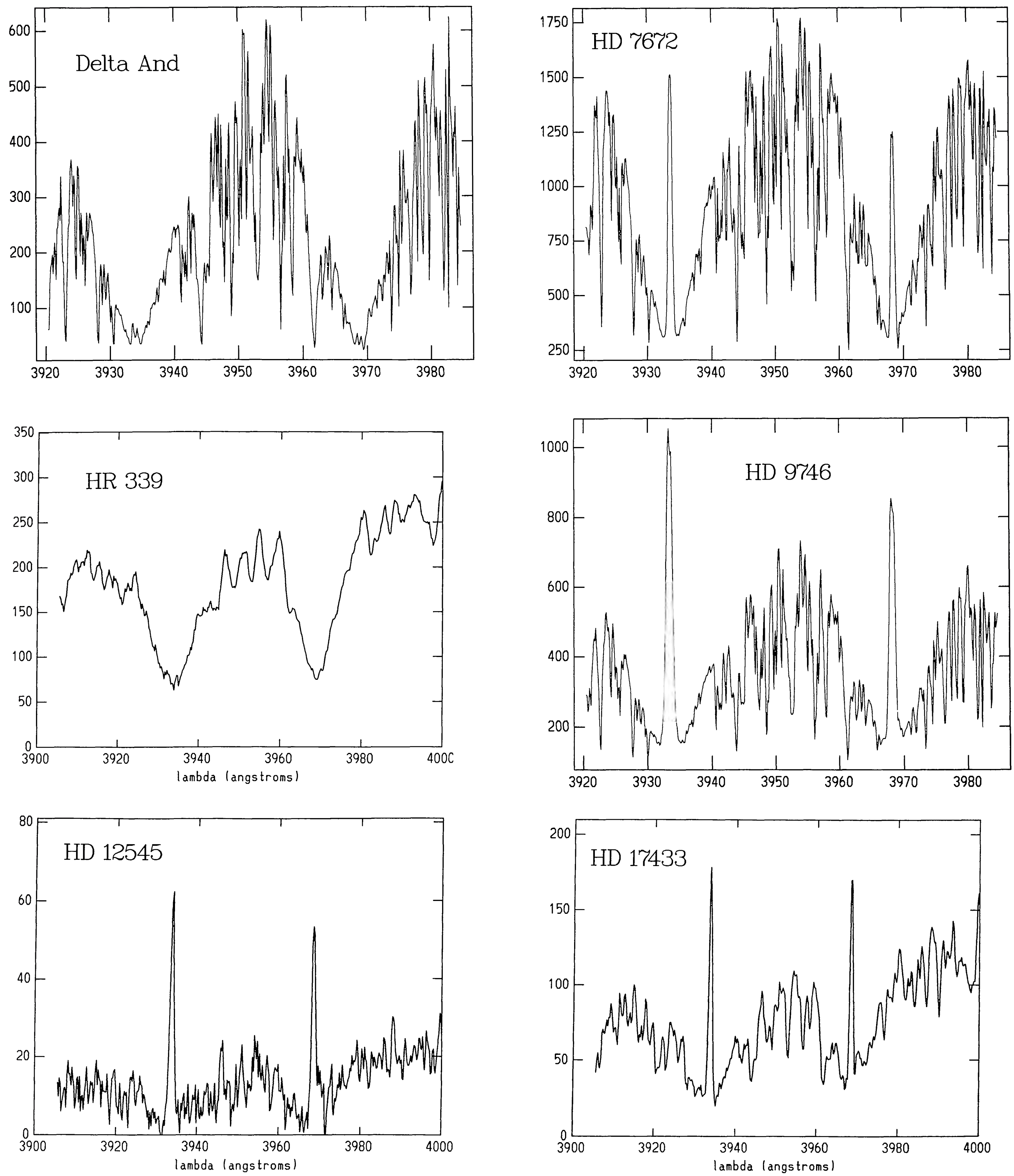

FIG. 10.—Individual Ca II H and K line profiles for the stars listed in Table 3 (representative examples)

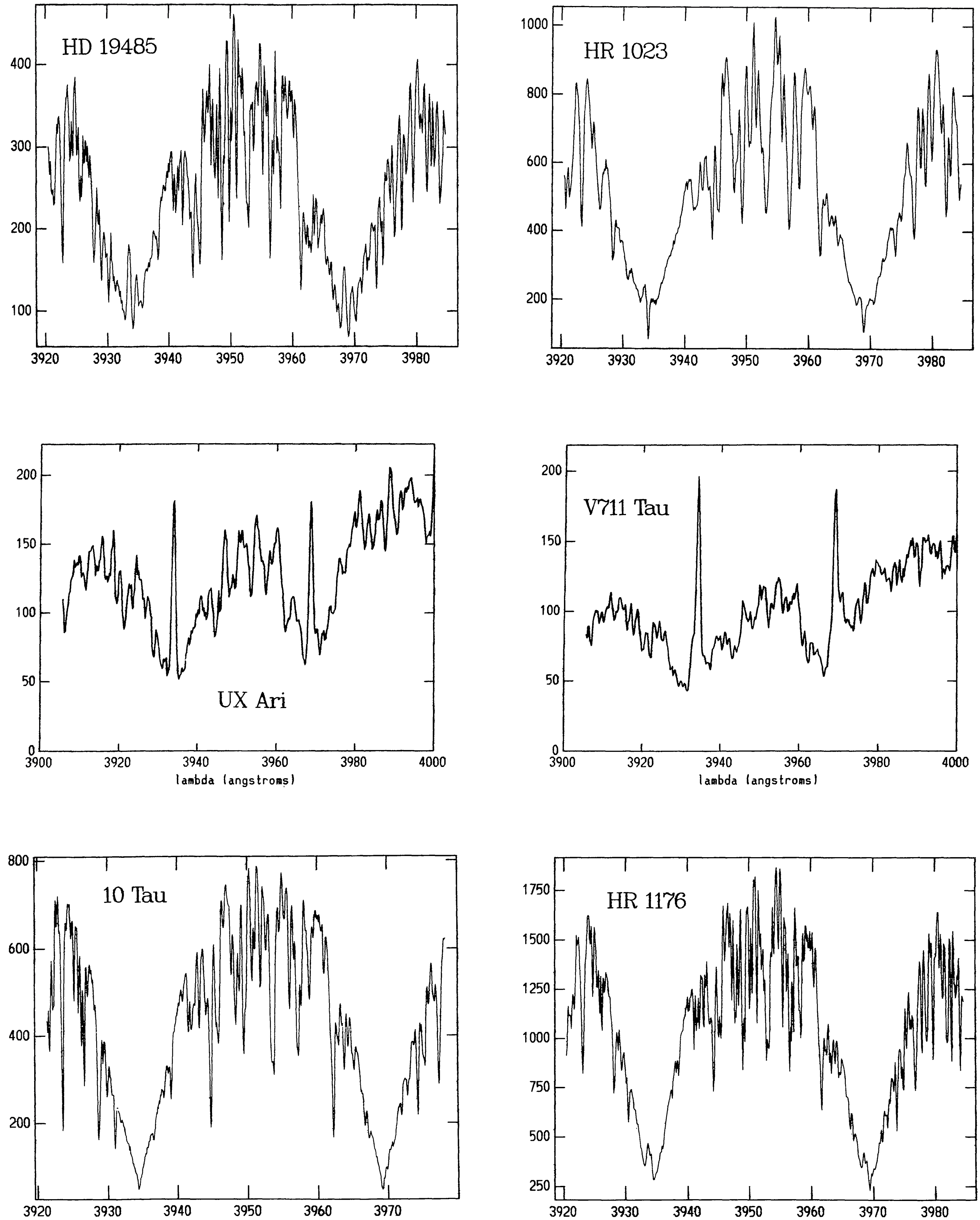

FIG. 10—*Continued*

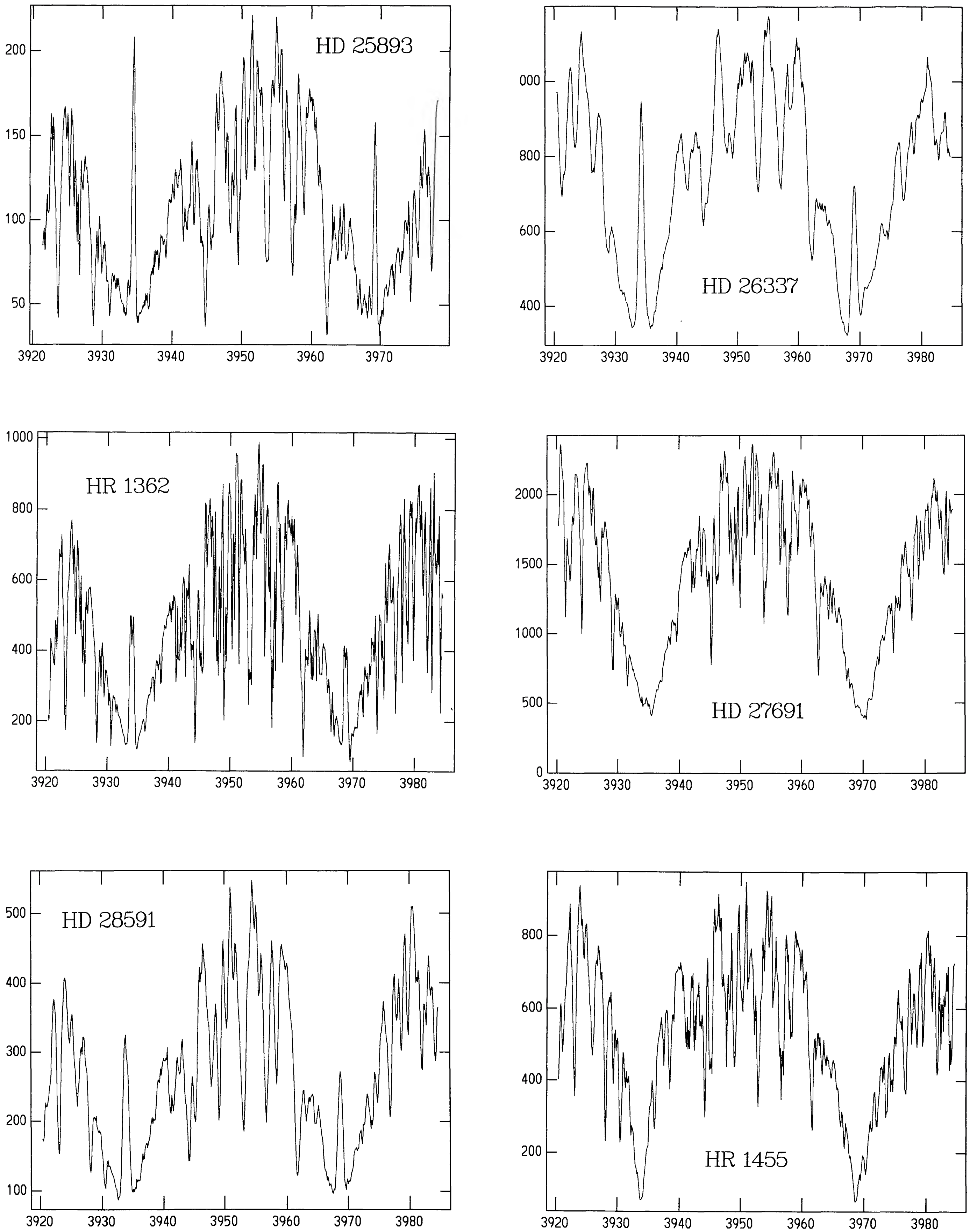

FIG. 10—*Continued*

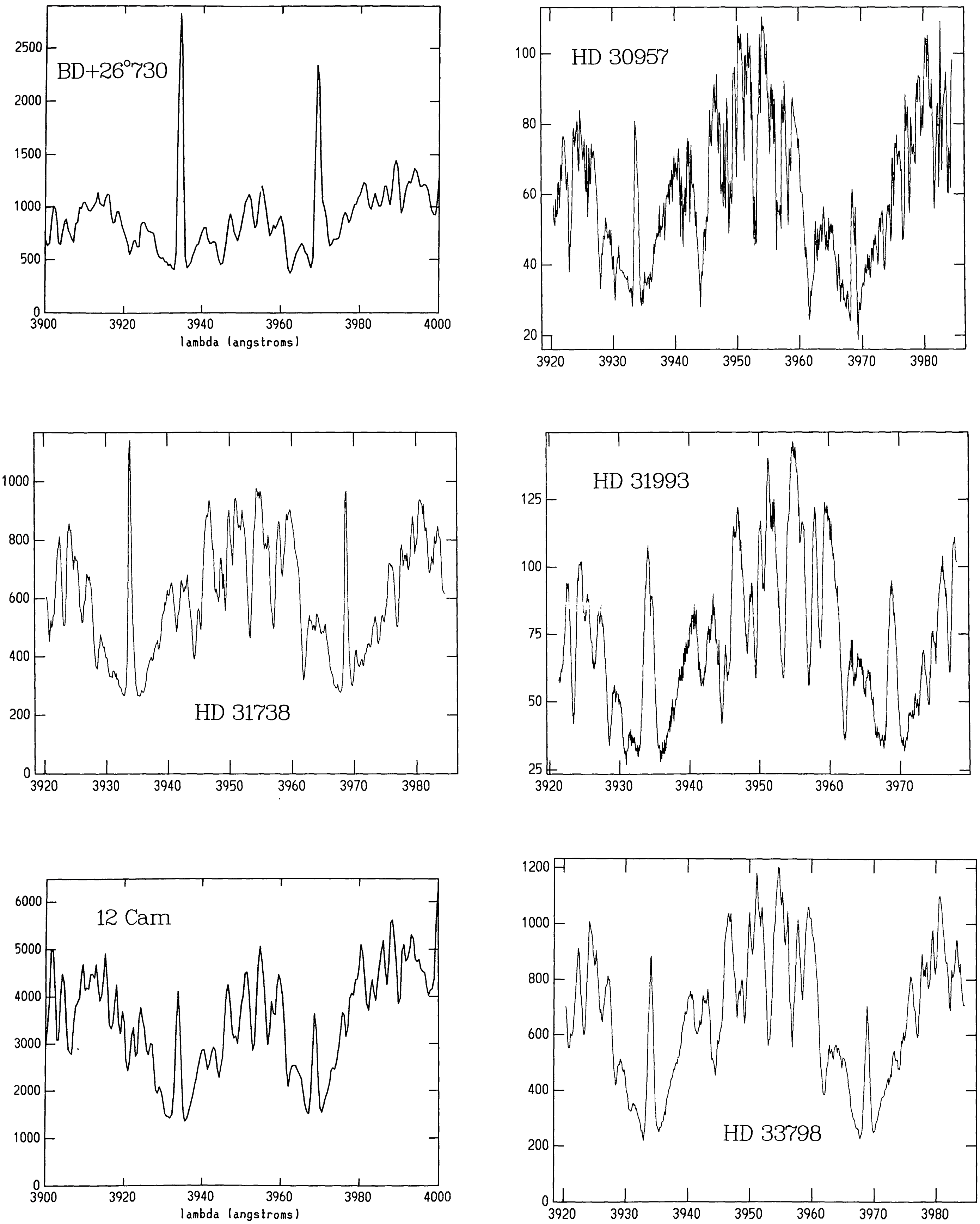

FIG. 10—*Continued*

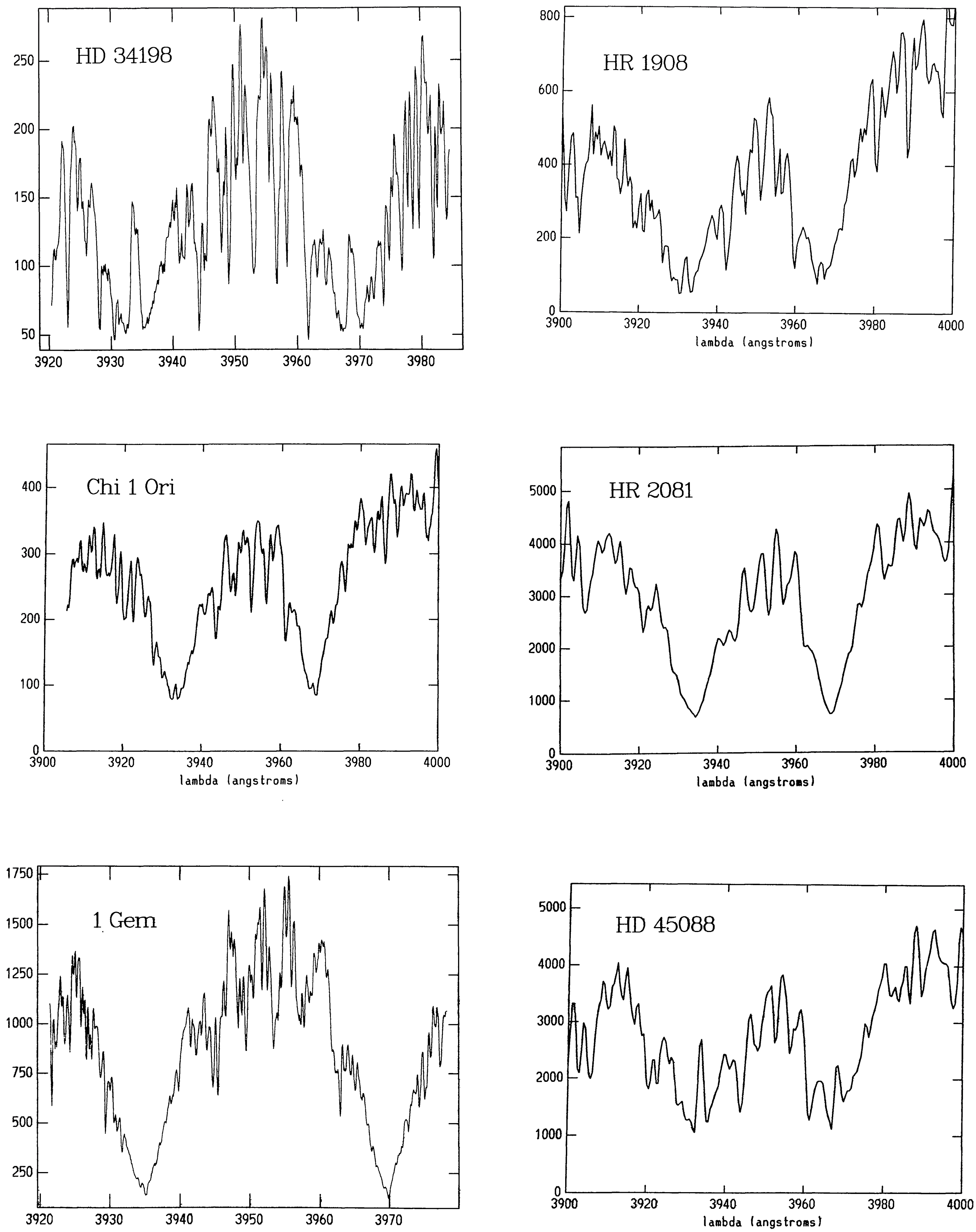

FIG. 10—*Continued*

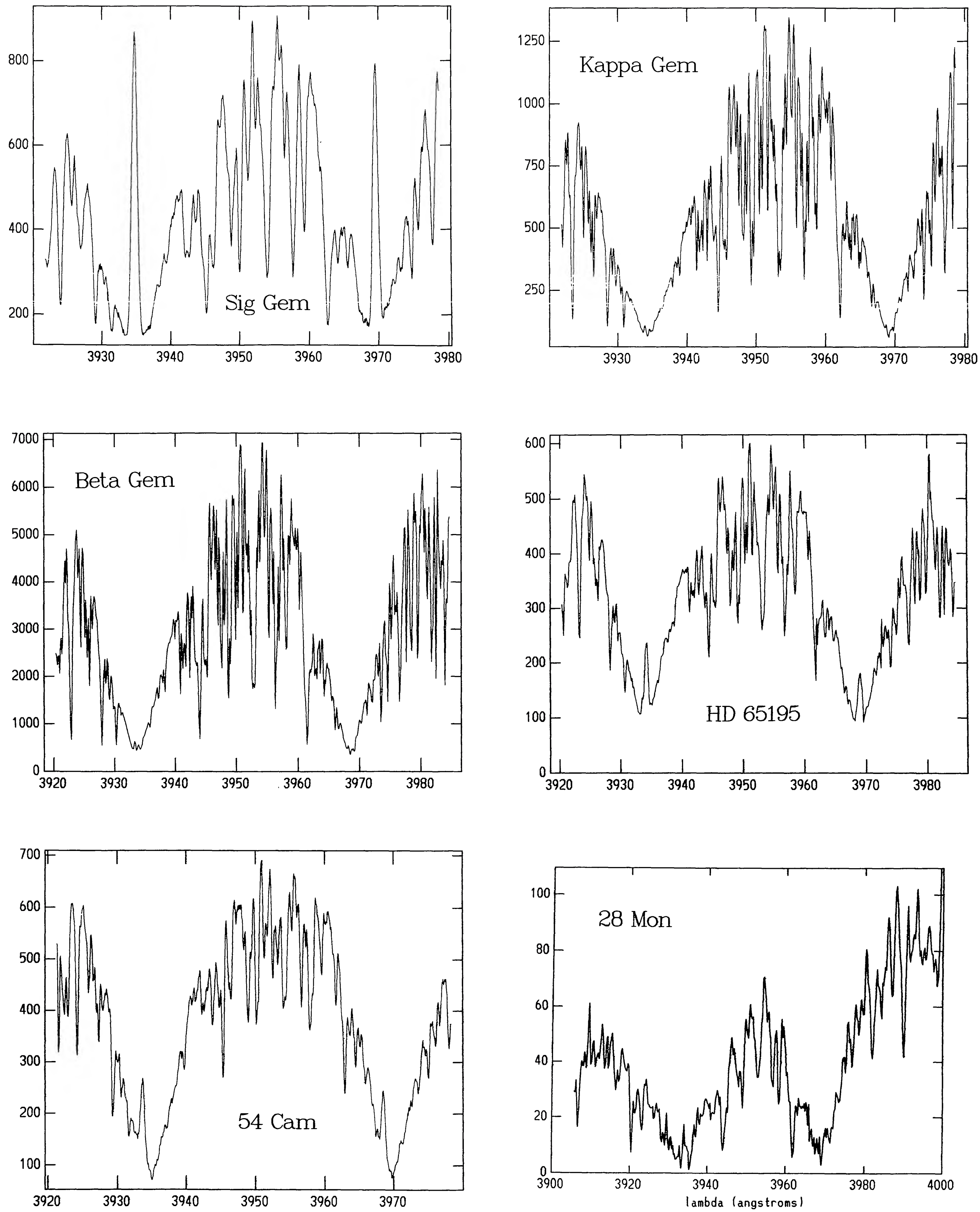

FIG. 10—*Continued*

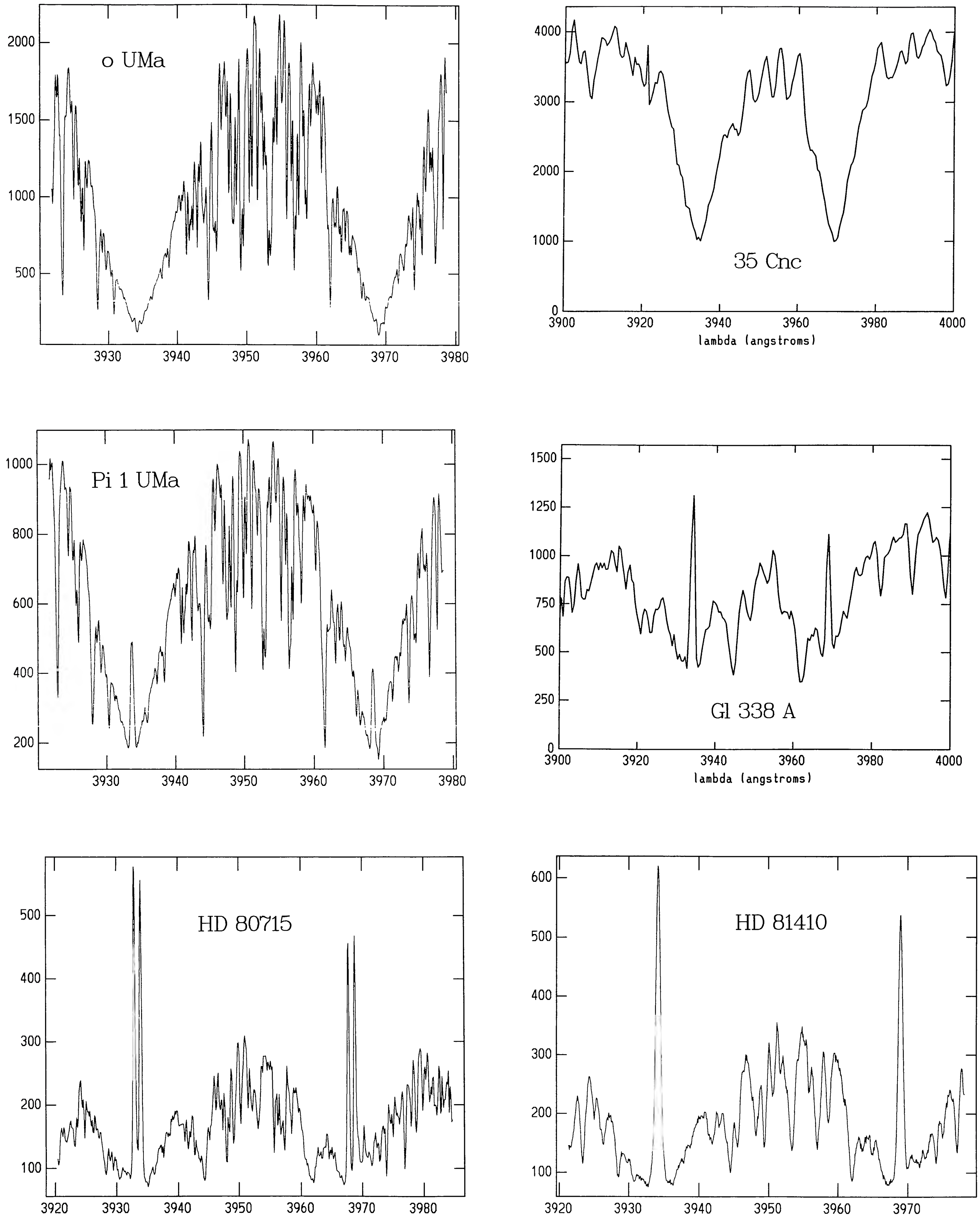

FIG. 10—*Continued*

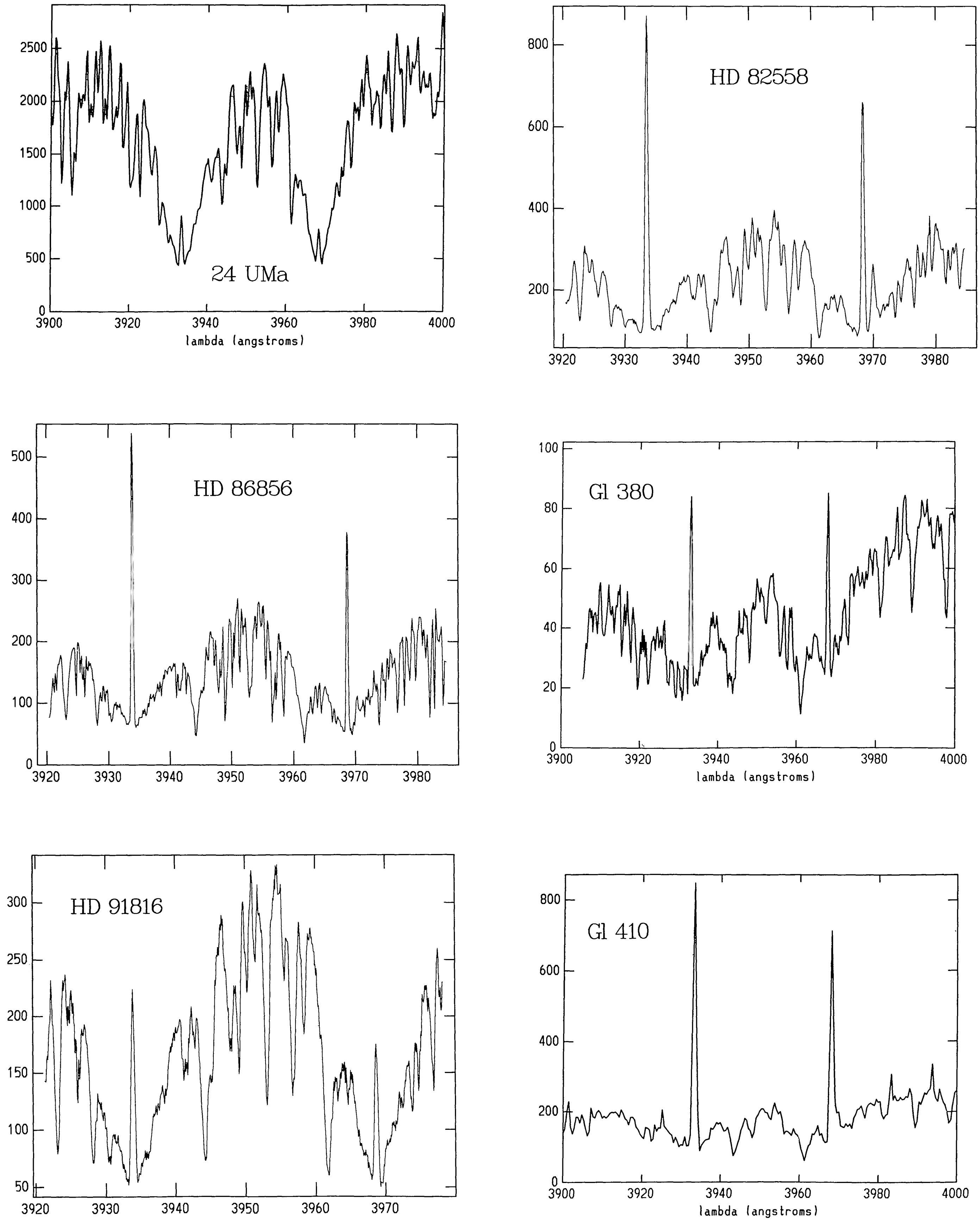

FIG. 10—*Continued*

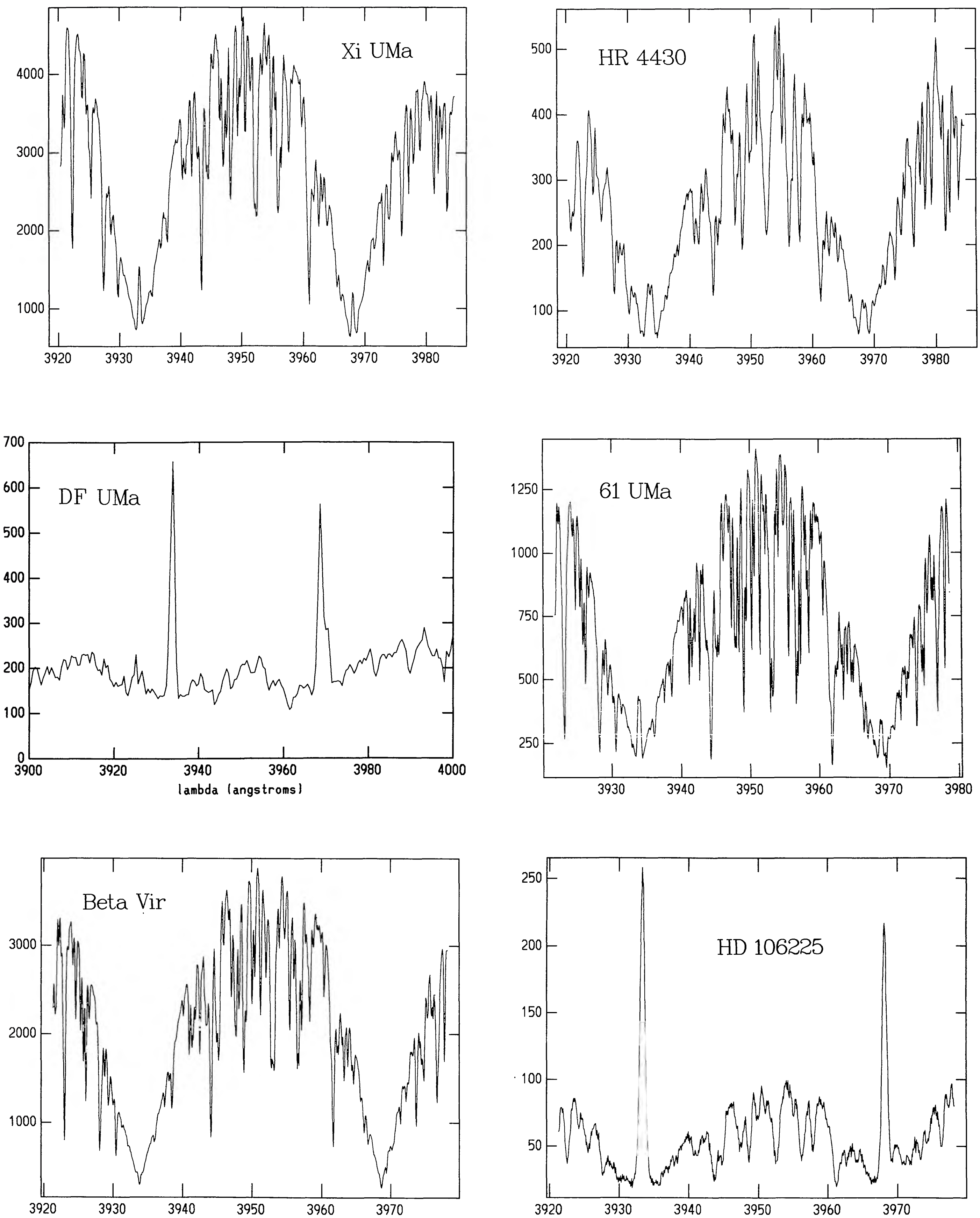

FIG. 10—*Continued*

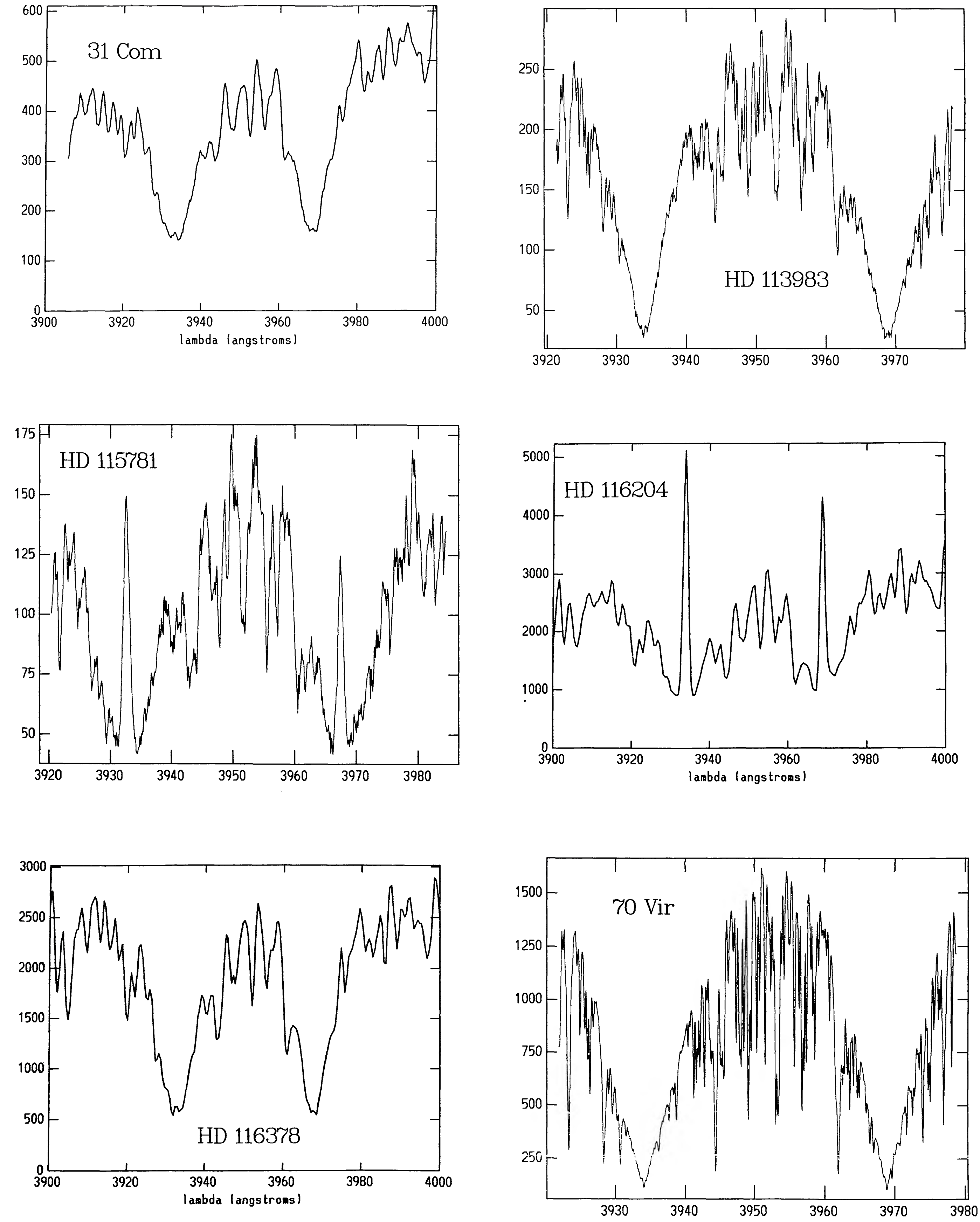

FIG. 10—*Continued*

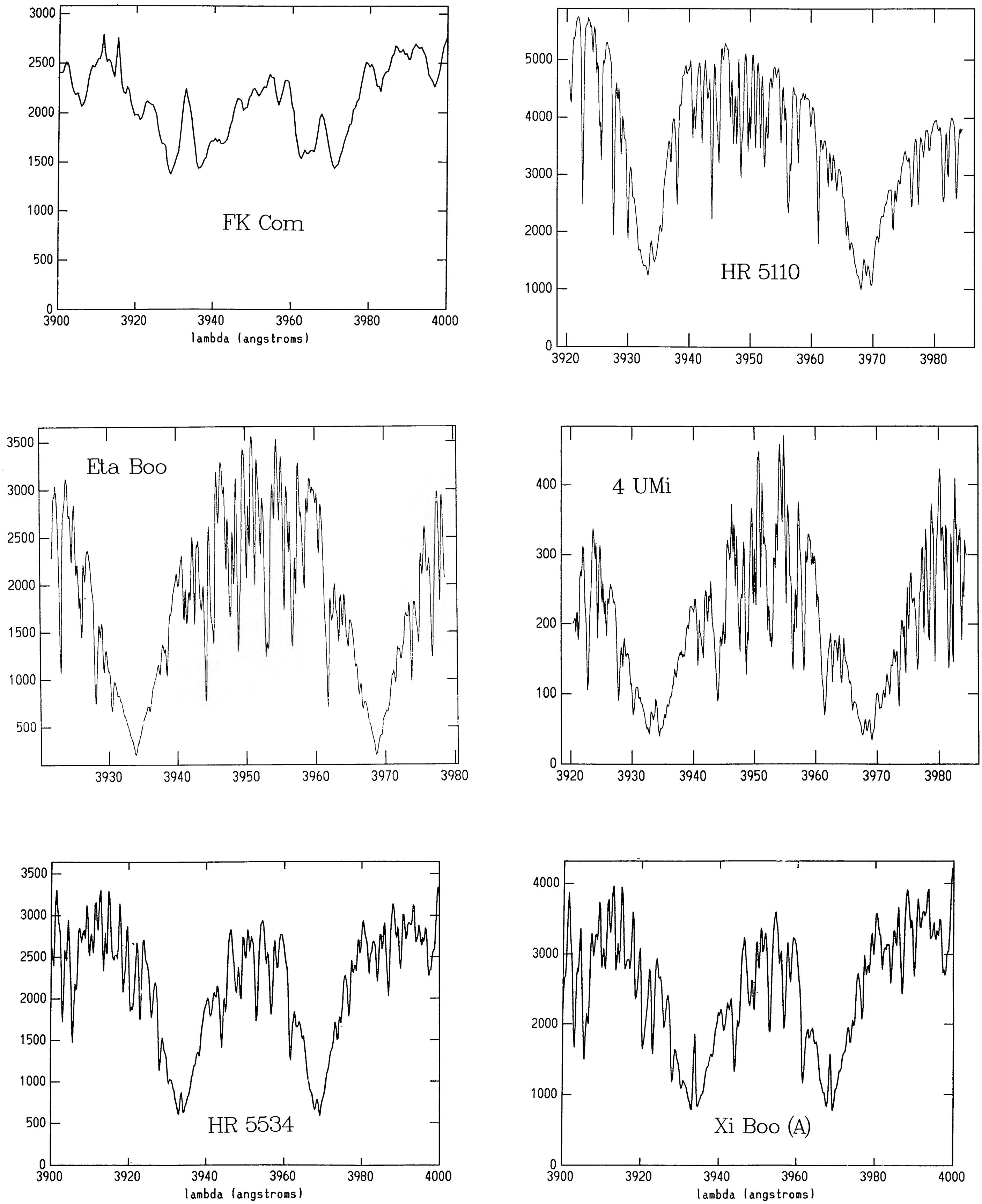

FIG. 10—*Continued*

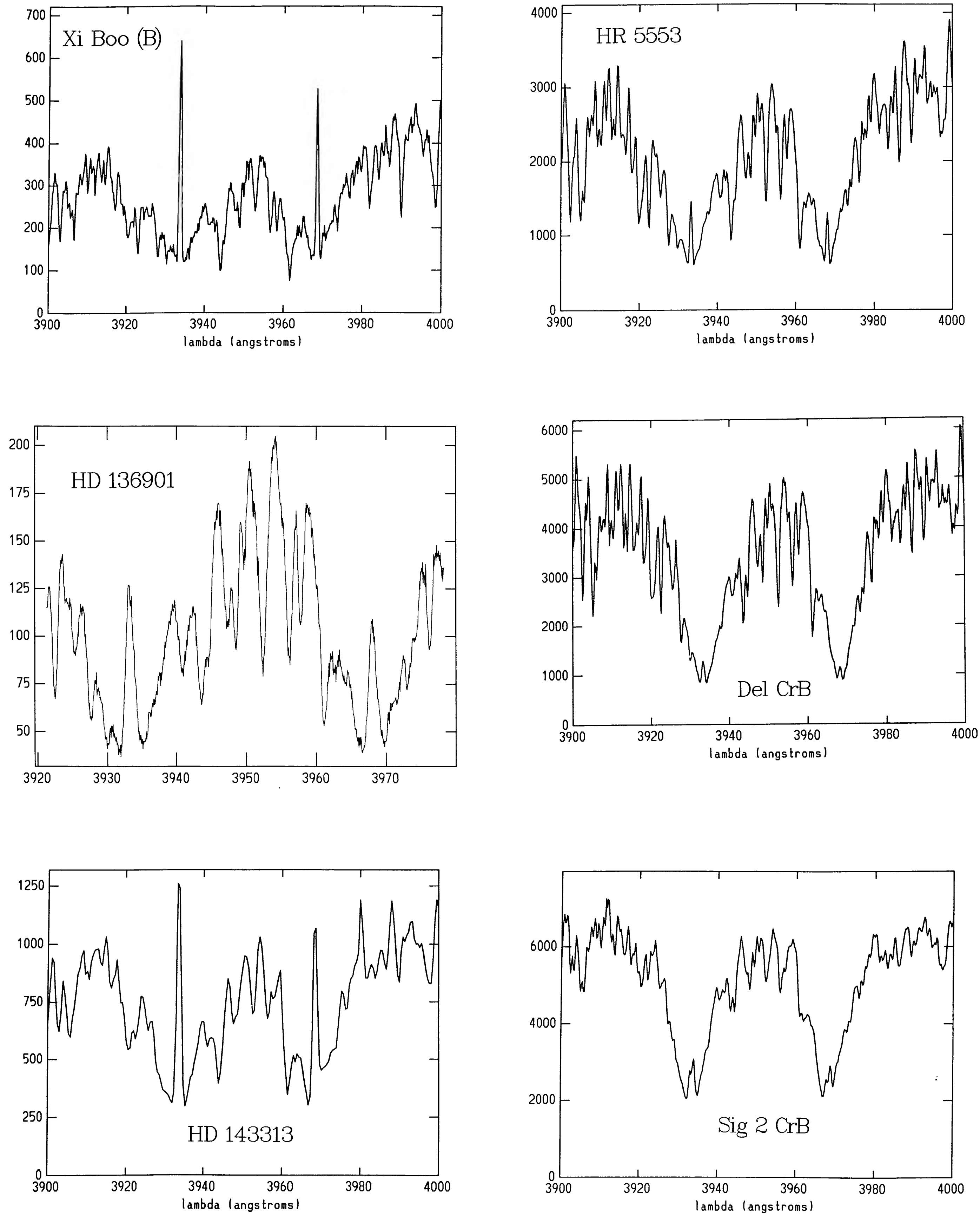

FIG. 10—*Continued*

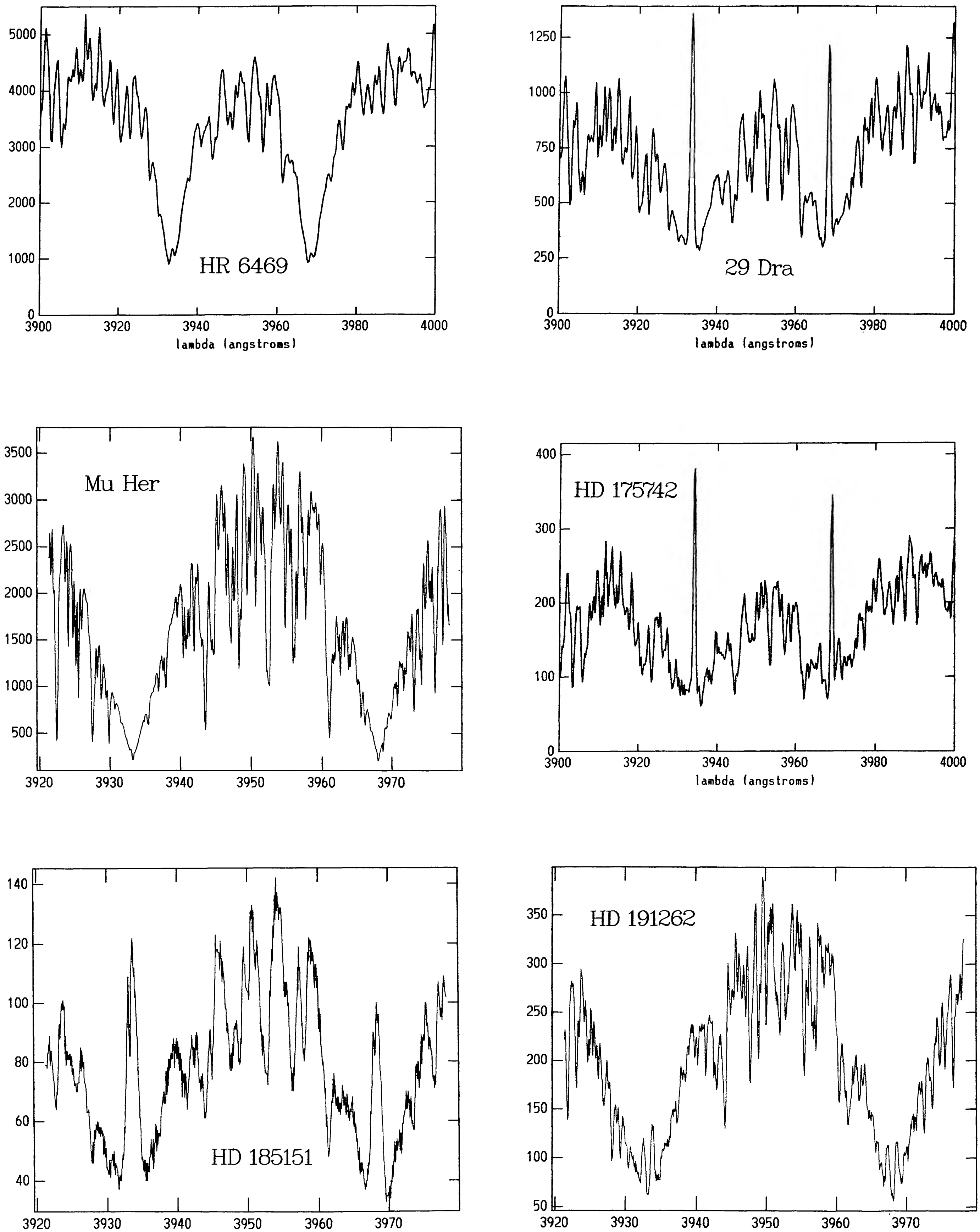

FIG. 10—*Continued*

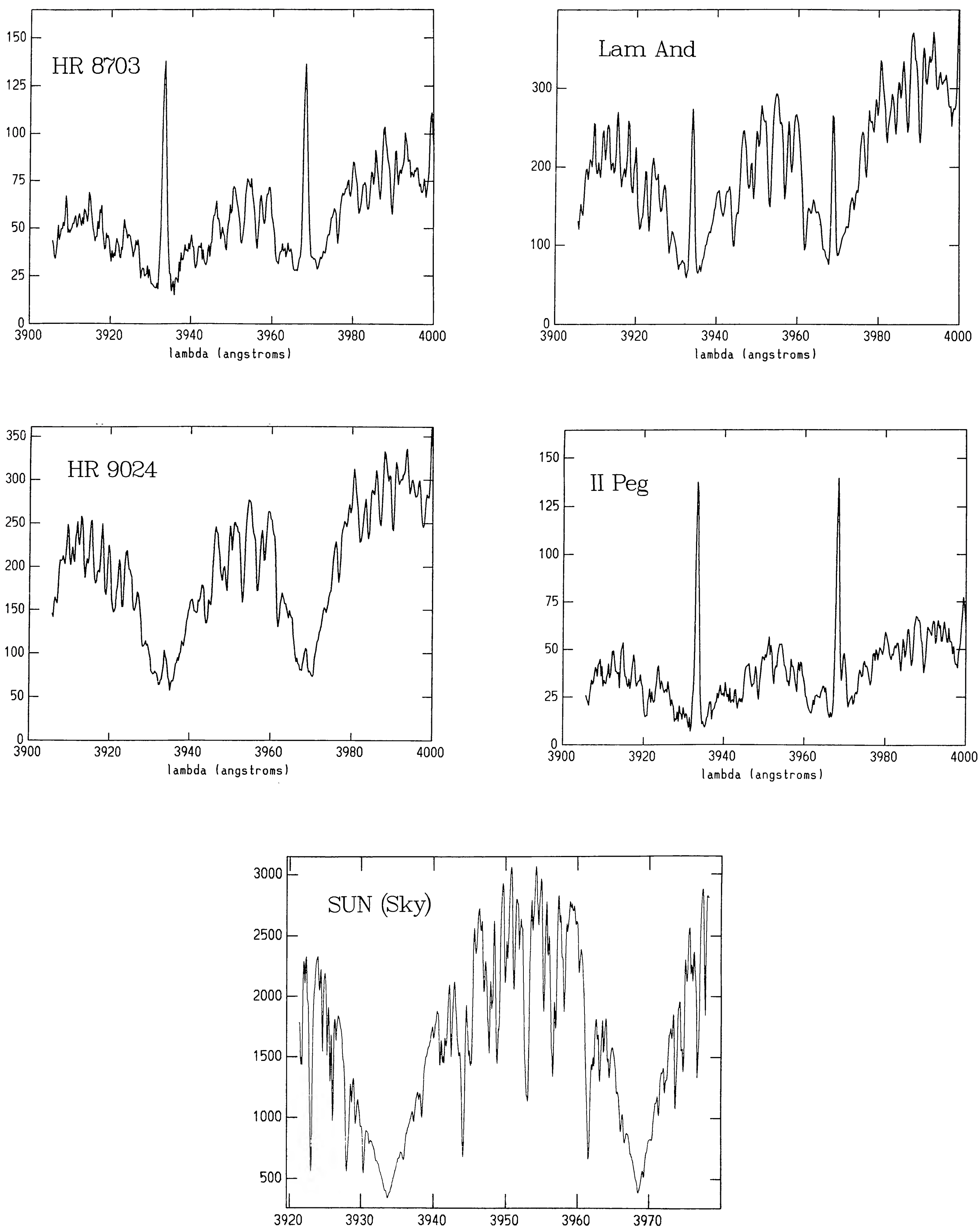

FIG. 10—*Continued*

REFERENCES

Baliunas, S. L., *et al.* 1983, *Ap. J.*, **275**, 752.
Barden, S. C. 1985, *Ap. J.*, **295**, 162.
Barden, S. C., and Nations, H. L. 1988, private communication.
Barnes, T. G., and Evans, D. S. 1976, *M.N.R.A.S.*, **174**, 489.
Basri, G. 1987, *Ap. J.*, **316**, 377.
Basri, G., Laurent, R., and Walter, F. M. 1985, *Ap. J.*, **298**, 761.
Beavers, W. I., and Griffin, R. F. 1979, *Pub. A.S.P.*, **91**, 824.
Bopp, B. W. 1983, in *IAU Colloquium 71, Activity in Red Dwarf Stars*, ed. P. B. Byrne and M. Rodonó (Dordrecht: Reidel), p. 363.
______. 1984, *Ap. J. Suppl.*, **54**, 387.
Bopp, B. W., Africano, J. L., Stencel, R. E., Noah, P. V., and Klimke, A. 1983, *Ap. J.*, **275**, 691.
Bopp, B. W., Ake, T. B., Goodrich, B. D., Africano, J. L., Noah, P. V., Meredith, R. J., Palmer, L. H., and Quigley, R. 1985, *Ap. J.*, **297**, 691.
Bopp, B. W., Dempsey, R. C., and Maniak, S. 1988, *Ap. J. Suppl.*, **68**, 803.
Bopp, B. W., and Fekel, F. C. 1977, *A.J.*, **82**, 490.
Bopp, B. W., Saar, S. H., Ambruster, C., Feldman, P., Dempsey, R., Allen, M., and Barden, S. C. 1989, *Ap. J.*, **339**, 1059.
Campbell, B. 1984, *Ap. J.*, **283**, 209.
Cayrel, R., Cayrel de Strobel, G., Campbell, B., Mein, N., Mein, P., and Dumont, S. 1983, *Astr. Ap.*, **123**, 89.
Cram, L. E., and Giampapa, M. S. 1987, *Ap. J.*, **323**, 316.
Deslandres, H. A,. and Burson, V. 1922, *C.R. Acad. Sci., Paris*, **175**, 121.
Duncan, D. K. 1981, *Ap. J.*, **248**, 651.
______. 1984, in *Cool Stars, Stellar Systems, and the Sun*, ed. S. L. Baliunas and L. Hartmann (Berlin: Springer), p. 128.
Eberhard, G., and Schwarzschild, K. 1913, *Ap. J.*, **38**, 292.
Fekel, F. C., Moffett, T. J., and Henry, G. W. 1986, *Ap. J. Suppl.*, **60**, 551.
Fernández-Figueroa, M. J., de Castro, E., Montesinos, B., Barreiro, F. J., Giménez, A., and Reglero, V. 1986*a*, *Adv. Space Res.*, **6**, 187.
Fernández-Figueroa, M. J., Montesinos, B., de Castro, E., Rego, M., Giménez, A., and Reglero, V. 1986*b*, *Astr. Ap.*, **169**, 219.
Giampapa, M. S., Worden, S. P., Schneeberger, T. J., and Cram, L. E. 1981, *Ap. J.*, **246**, 502.
Gray, D. F. 1982, *Ap. J.*, **262**, 682.
Griffin, R. F., and Radford, G. A. 1976, *Observatory*, **96**, 188.
Hartmann, L., Soderblom, D. R., Noyes, R. W., Burnham, N., and Vaughan, A. H. 1984, *Ap. J.*, **276**, 254.
Herbig, G. H. 1985, *Ap. J.*, **289**, 269.
Johnson, H. L. 1966, *Ann. Rev. Astr. Ap.*, **4**, 193.
Keenan, P. C. 1983, *Bull. Information CDS*, No. 24, p. 19.
Kelch, W. L., Linsky, J. L., and Worden, S. P. 1979, *Ap. J.*, **229**, 700.
Linsky, J.L., and Ayres, T. R. 1978, *Ap. J.*, **220**, 619.
Linsky, J. L., Worden, S. P., McClintock, W., and Robertson, R. M. 1979, *Ap. J. Suppl.*, **41**, 47.
Lloyd-Evans, T. 1987, *S.A.A.O. Circ.*, No. 11, p. 73.
Middelkoop, F. 1982, *Astr. Ap.*, **107**, 31.
Noyes, R. W., Hartmann, L. W., Baliunas, S. L., Duncan, D. K., and Vaughan, A. H. 1984, *Ap. J.*, **279**, 763.
Pasquini, L., Pallavicini, R., and Pakull, M. 1988, *Astr. Ap.*, **191**, 253.
Pilachowski, C., and Barnes, J. 1987, *IRAF Reduction of Coudé/CCD Spectra* (Tucson: NOAO/KPNO).
Rutten, R. G. M. 1987, *Astr. Ap.*, **177**, 131.
Rutten, R. G. M., and Schrijver, C. J. 1987, *Astr. Ap.*, **177**, 155.
Schmidt-Kaler, T. 1982, in *Landolt-Börnstein*, Vol. **2b**, ed. K. Schaifers and H. H. Voigt (Heidelberg: Springer), p. 1.
Simon, T., and Fekel, F. C. 1987, *Ap. J.*, **316**, 434.
Simon, T., Herbig, G., and Boesgaard, A. M. 1985, *Ap. J.*, **293**, 551.
Smith, S. E. 1984, Ph.D. thesis, The University of Toledo.
Smith, S. E., and Bopp, B. W. 1982, *Ap. Letters*, **22**, 127.
Soderblom, D. R. 1985, *A.J.*, **90**, 2103.
______. 1989, *Ap. J.*, **342**, 823.
Stern, R. A., Nousek, J. A., Nugent, J. J., Agrawal, P. C., Riegler, G. R., Rosenthal, A., Pravdo, S. H., and Garmire, G. P. 1981, *Ap. J. (Letters)*, **251**, L105.
Strassmeier, K. G., and Hall, D. S. 1988, *Ap. J. Suppl.*, **67**, 453.
Strassmeier, K. G., Hall, D. S., Boyd, L. J., and Genet, R. M. 1989, *Ap. J. Suppl.*, **69**, 141.
Strassmeier, K. G., Hall, D. S., Zeilik, M., Nelson, E., Eker, Z., and Fekel, F. C. 1988, *Astr. Ap. Suppl.*, **72**, 291.
Strassmeier, K. G., Weichinger, S., and Hanslmeier, A. 1986, *Inf. Bull. Var. Stars*, No. 2937.
Tomkin, J. 1980, *A.J.*, **85**, 294.
Uesugi, A., and Fukuda, I. 1982, *Revised Catalog of Stellar Rotational Velocities* (Kyoto: Kyoto University).
Vaughan, A. H., and Preston, G. W. 1980, *Pub. A.S.P.*, **92**, 385.
Vogt, S. S. 1981, *Ap. J.*, **247**, 975.
Walter, F. M., and Basri, G. S. 1982, *Ap. J.*, **260**, 735.
Wellmann, P. 1940, *Zs. Ap.*, **19**, 236.
Willstrop, R. V. 1964, *Mem. R.A.S.*, **69**, 83.
Wolff, S. C., Boesgaard, A. M., and Simon, T. 1986, *Ap. J.*, **310**, 360.
Worden, S. P., Schneeberger, T. J., and Giampapa, M. S. 1981, *Ap. J. Suppl.*, **46**, 159.
Zarro, D. M., and Rodgers, A. W. 1983, *Ap. J. Suppl.*, **53**, 815.

BERNARD W. BOPP and ROBERT C. DEMPSEY: Department of Physics and Astronomy, University of Toledo, Toledo, OH 43606

FRANCIS C. FEKEL and KLAUS G. STRASSMEIER: Department of Physics and Astronomy, Vanderbilt University, Box 1807B, Nashville, TN 37235

GREGORY W. HENRY: Center of Excellence in Information Systems Engineering, Tennessee State University, 3500 John A. Merritt Boulevard, Nashville, TN 37209-1561